EURO KARST NEUCHÂTEL 2026

Field trip

Tsanfleuron-Sanetsch alpine karst system, water availability under climate change

03.09.26 - 04.09.26

Philippe Renard, Tangy Racine, Manon Trottet

Global overview of the Tsanfleuron area.

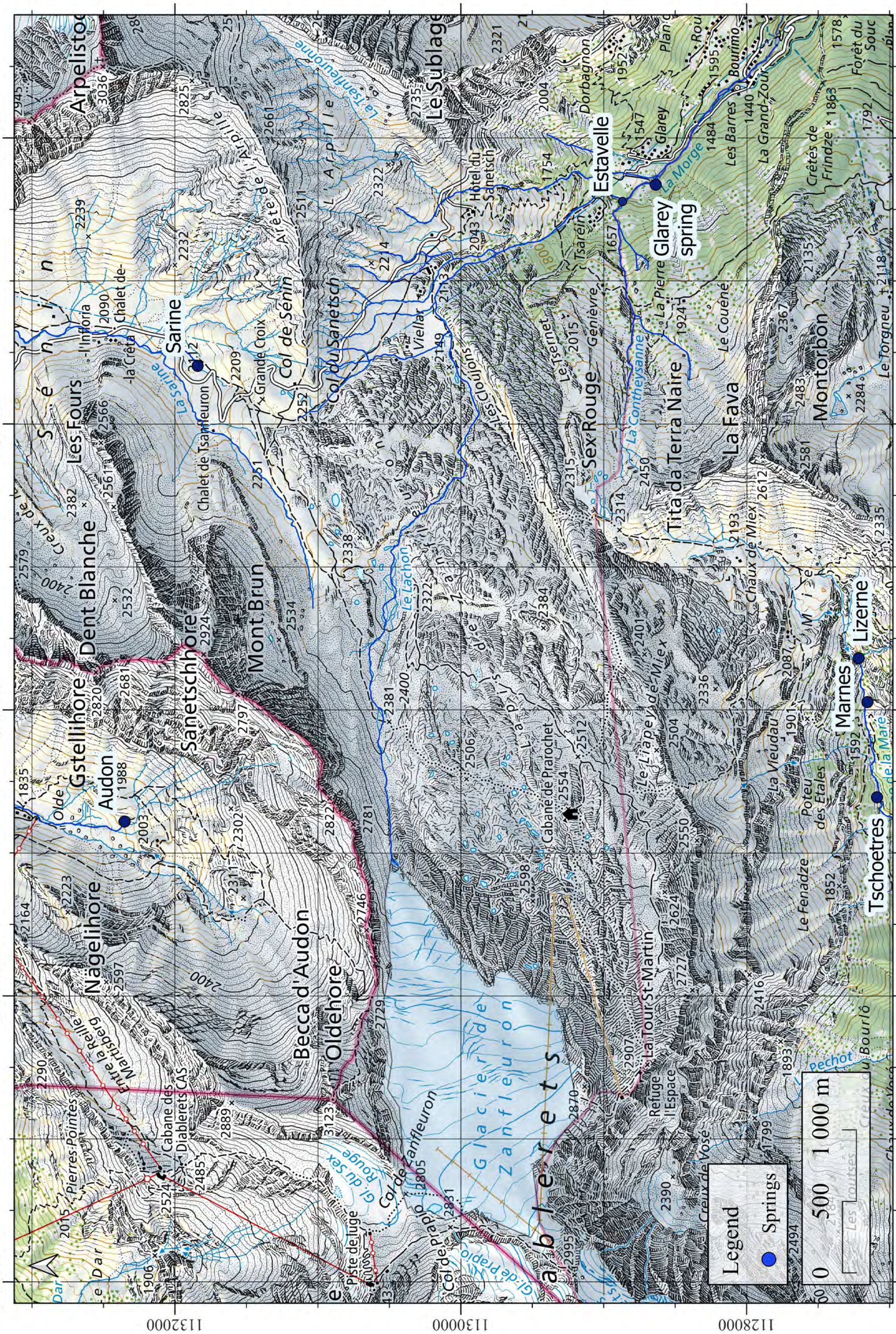

Topographic map of the Tsanfleuron region

Glarey spring. Collecting tunnel. Supplies drinking water to the municipalities of Conthey. Discharge ranges from 30 to 200 L/s.

Glarey spring and estavelle discharge.

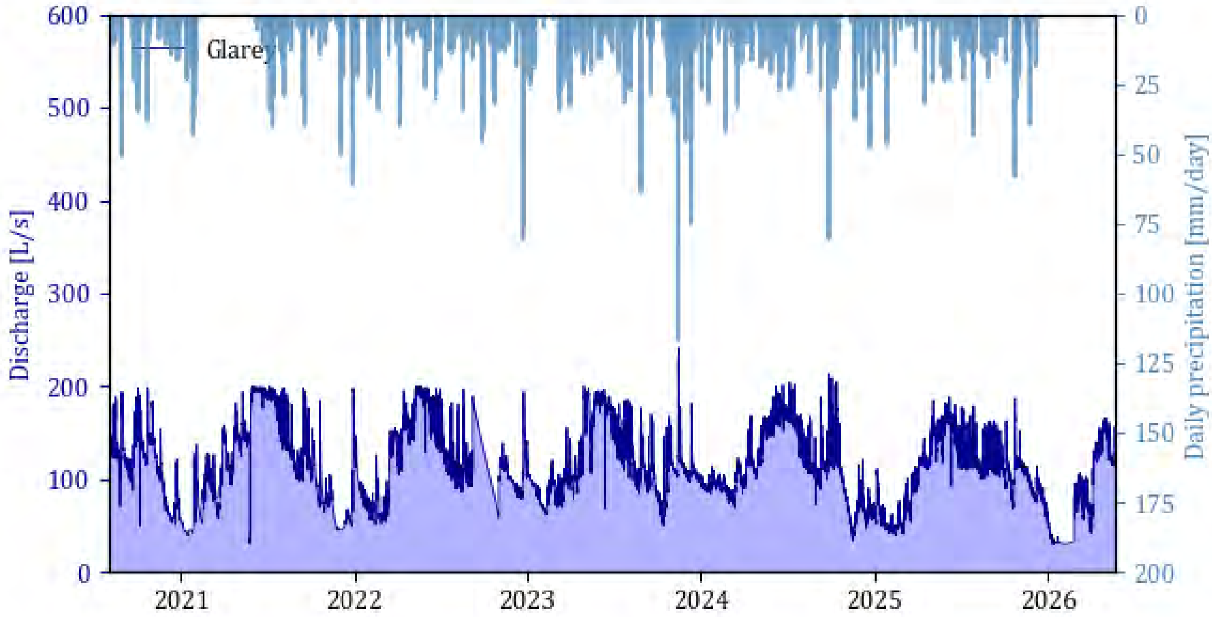

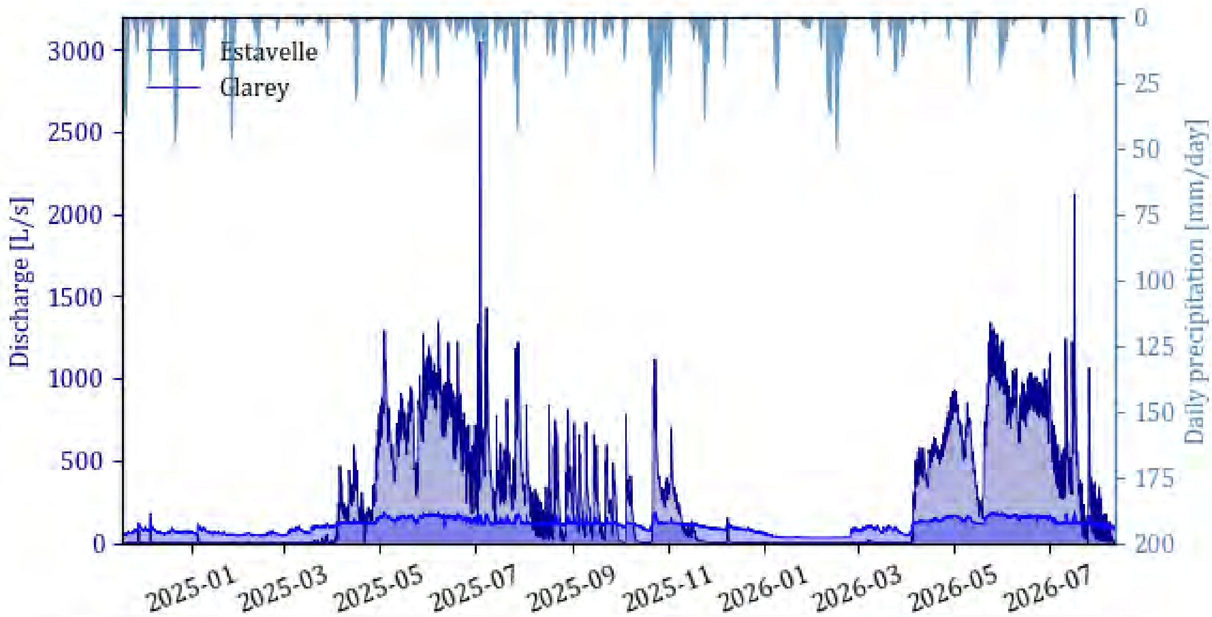

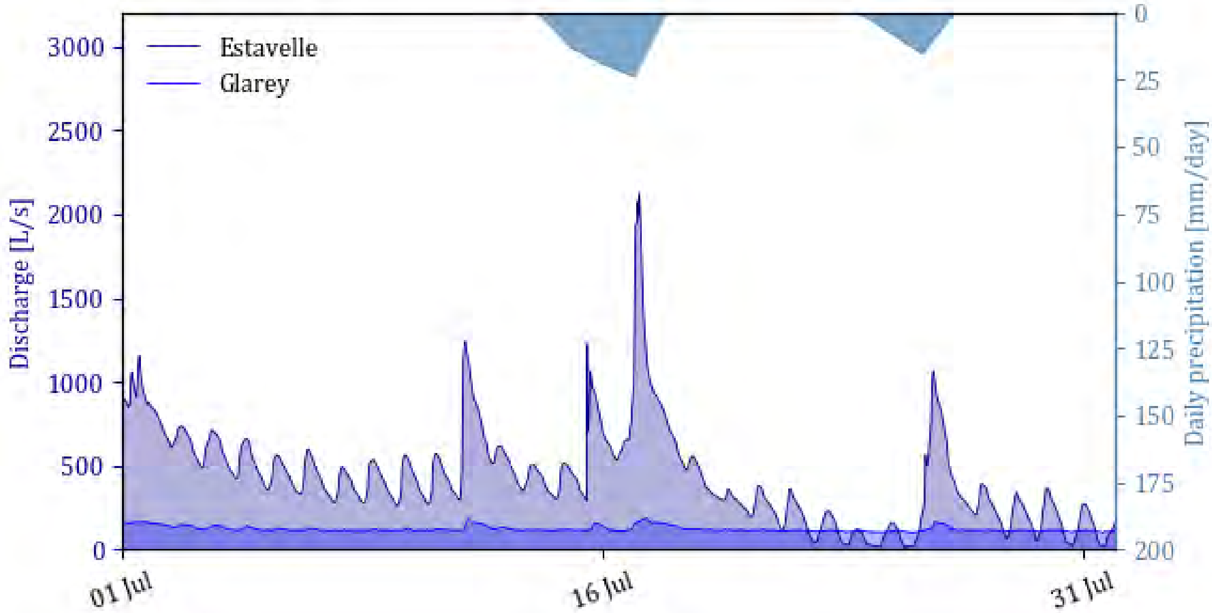

Simple reservoir model - simulated discharge at Glarey spring, obtained with the reservoir model developed (Salamin 2023)

RCP8.2

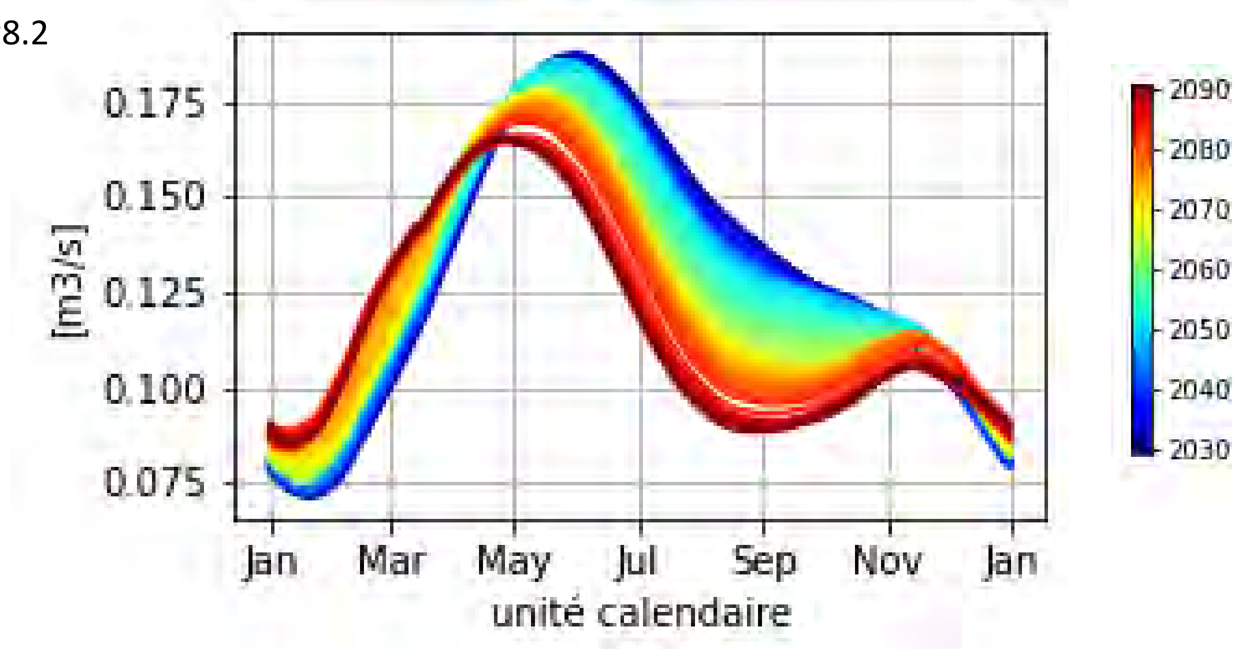

The values are smoothed using a 31-day and 15-year moving average.

Projected changes in annual discharge relative to 2022 for 2030, 2050, and 2090 under the RCP2.6, RCP4.5, and RCP8.5 scenarios. Violin plots show the distribution of the simulated changes across the different model projections; wider sections indicate a higher concentration of results.

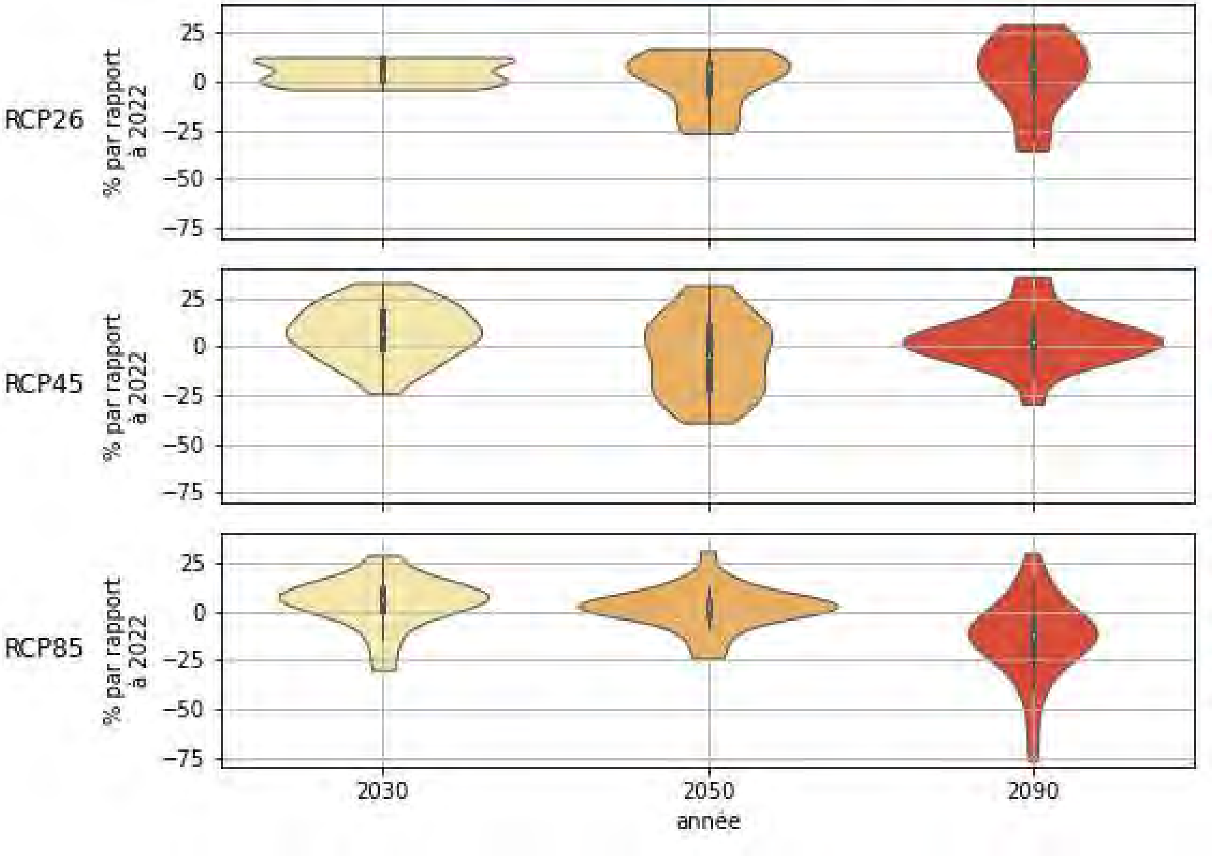

Water balance for 2021-2022 (Salamin 2023)

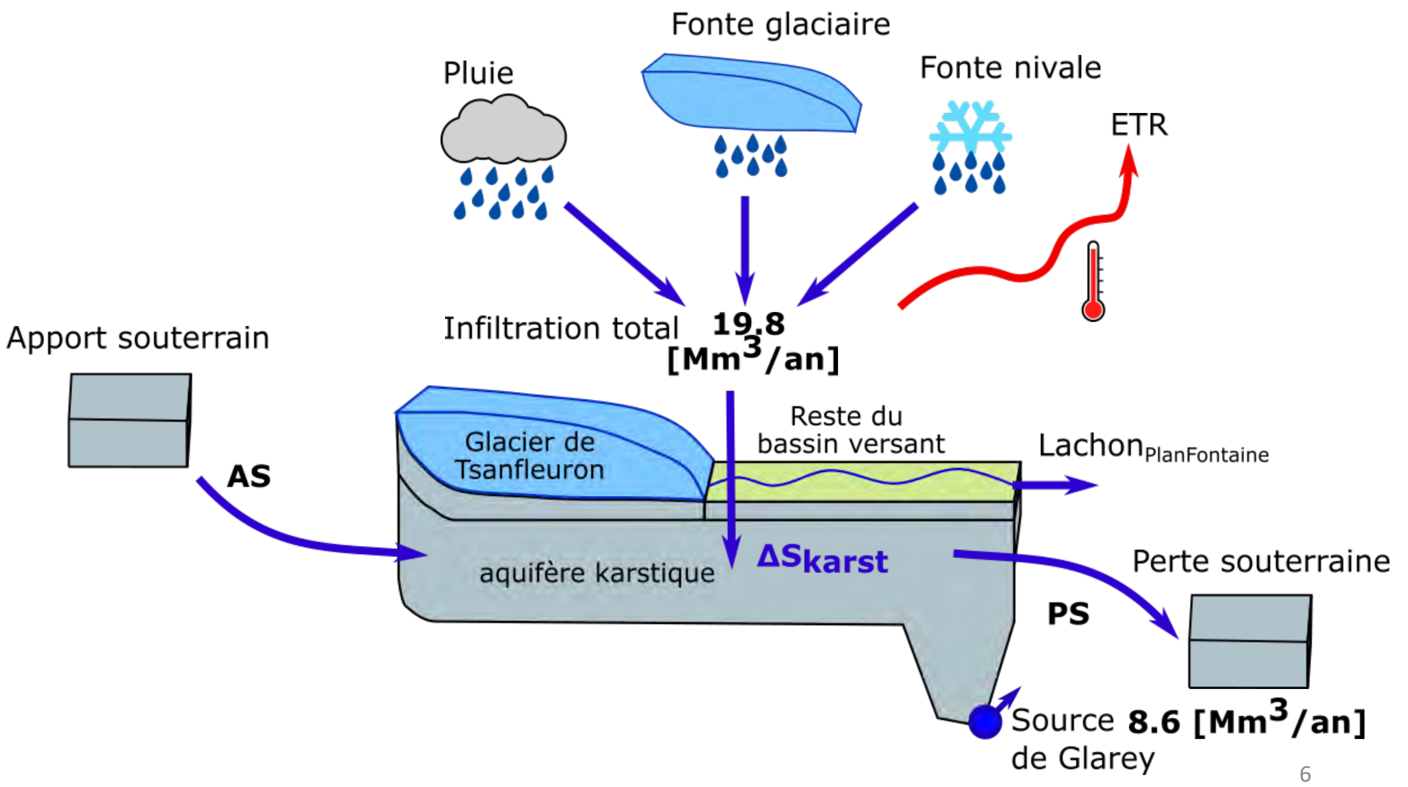

Overview of the Glarey area

Excavation of the Glarey estavelle in the 1990s (personal archives of Daniel Masotti).

Excavation of the Glarey estavelle in the 1990s (personal archives of Daniel Masotti).

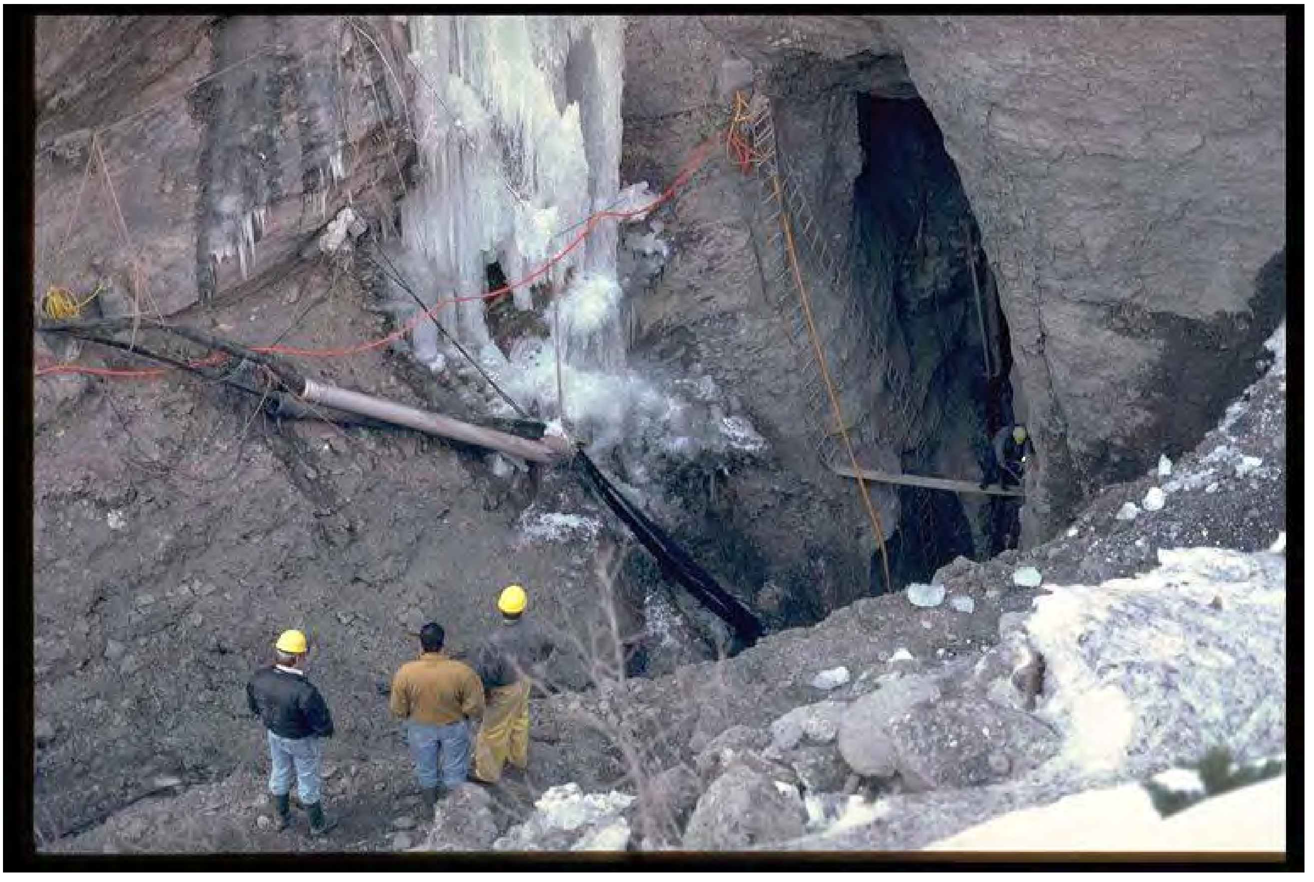

Aquifer type of Switzerland

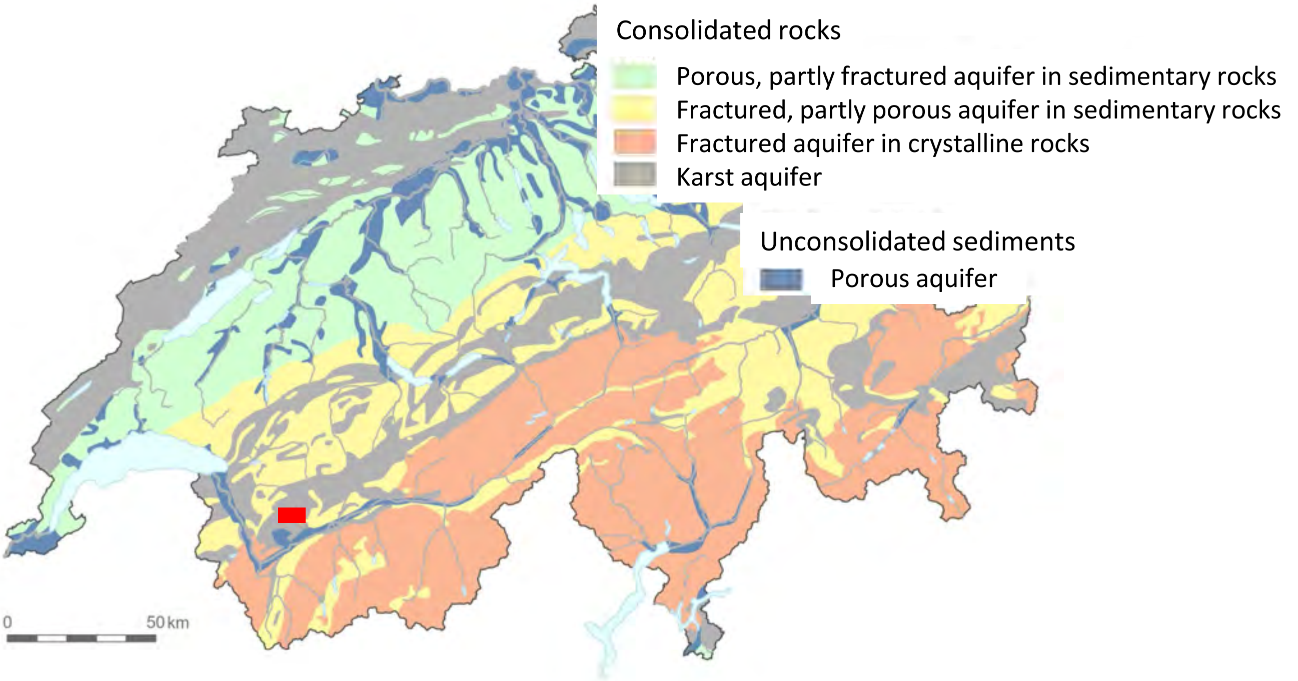

Tectonic sketch of Switzerland

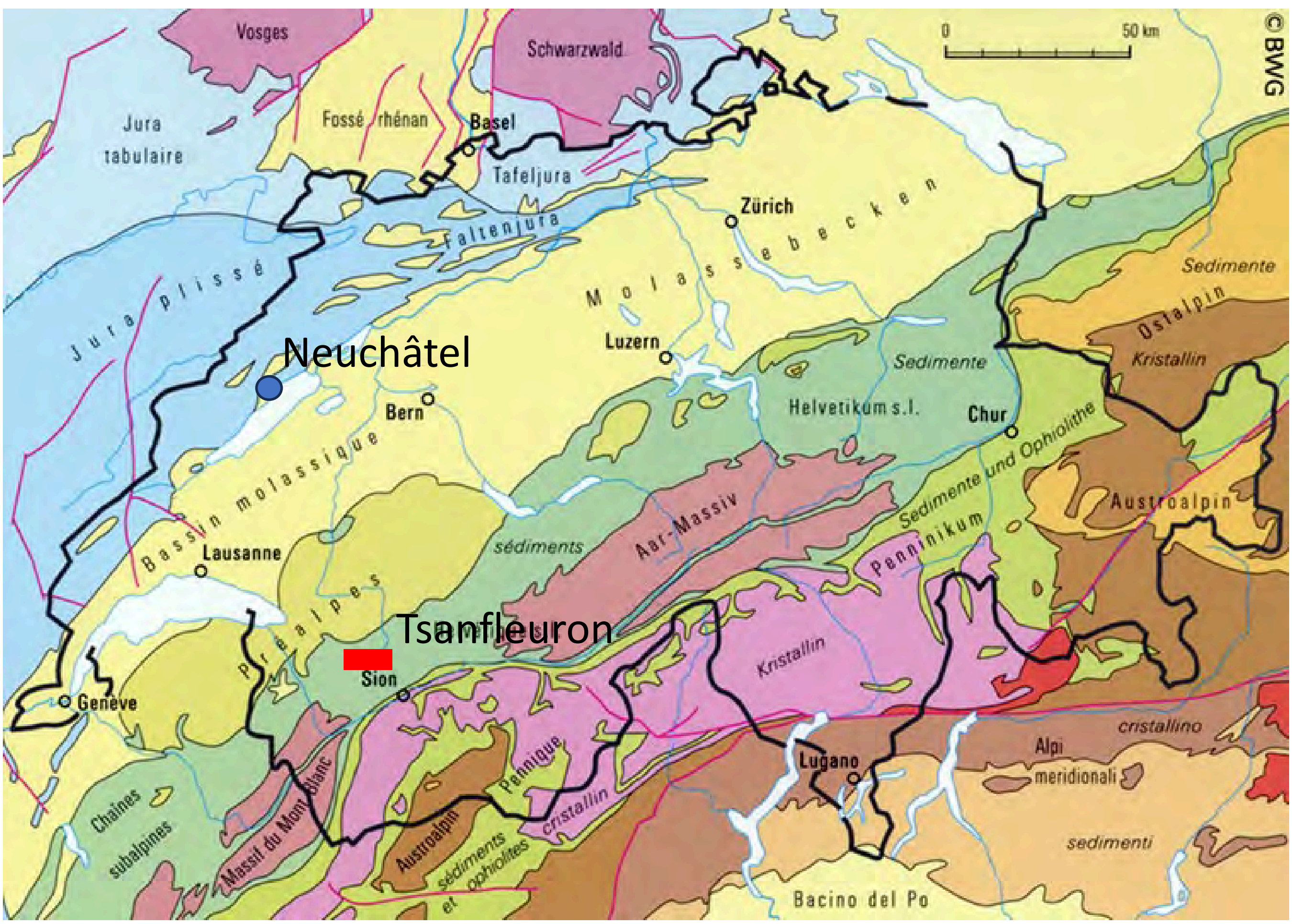

Simplified NW–SE tectonic cross-section of the Swiss Alps. The Tsanfleuron–Sanetsch area is located within the **Helvetic domain** of the Alps.

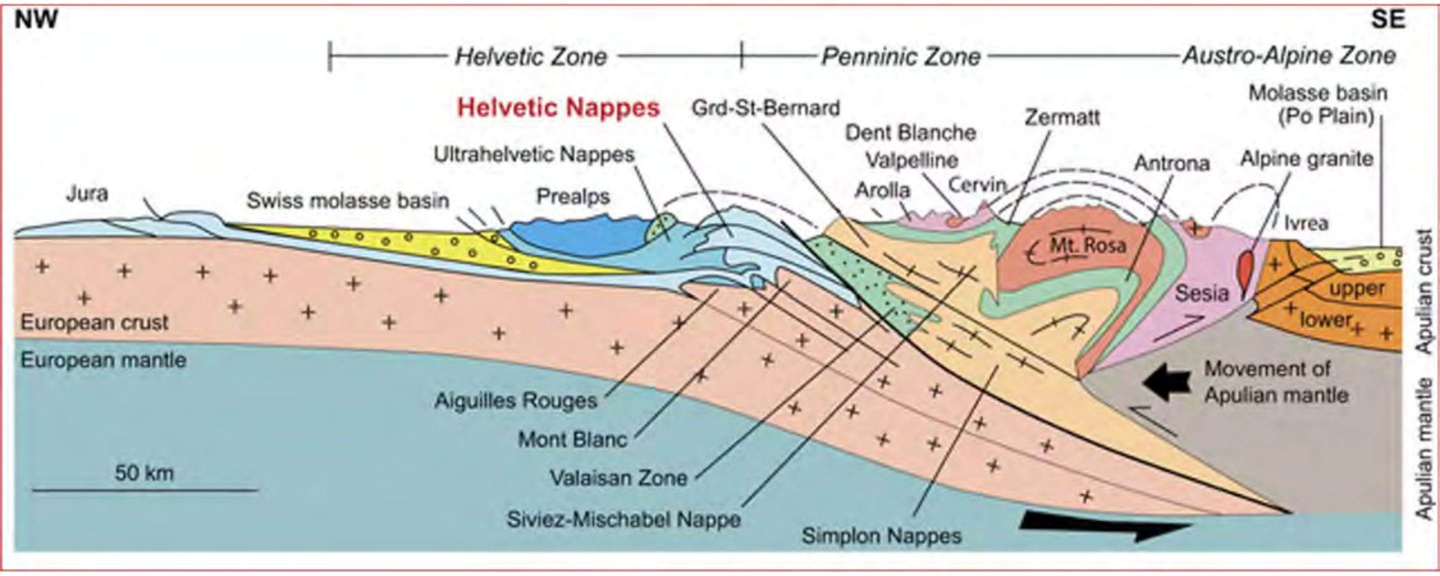

Cross section of the Helvetic nappe system in Western Switzerland (Schoeneich and Reynard 2020, modified by Epard, University of Lausanne).

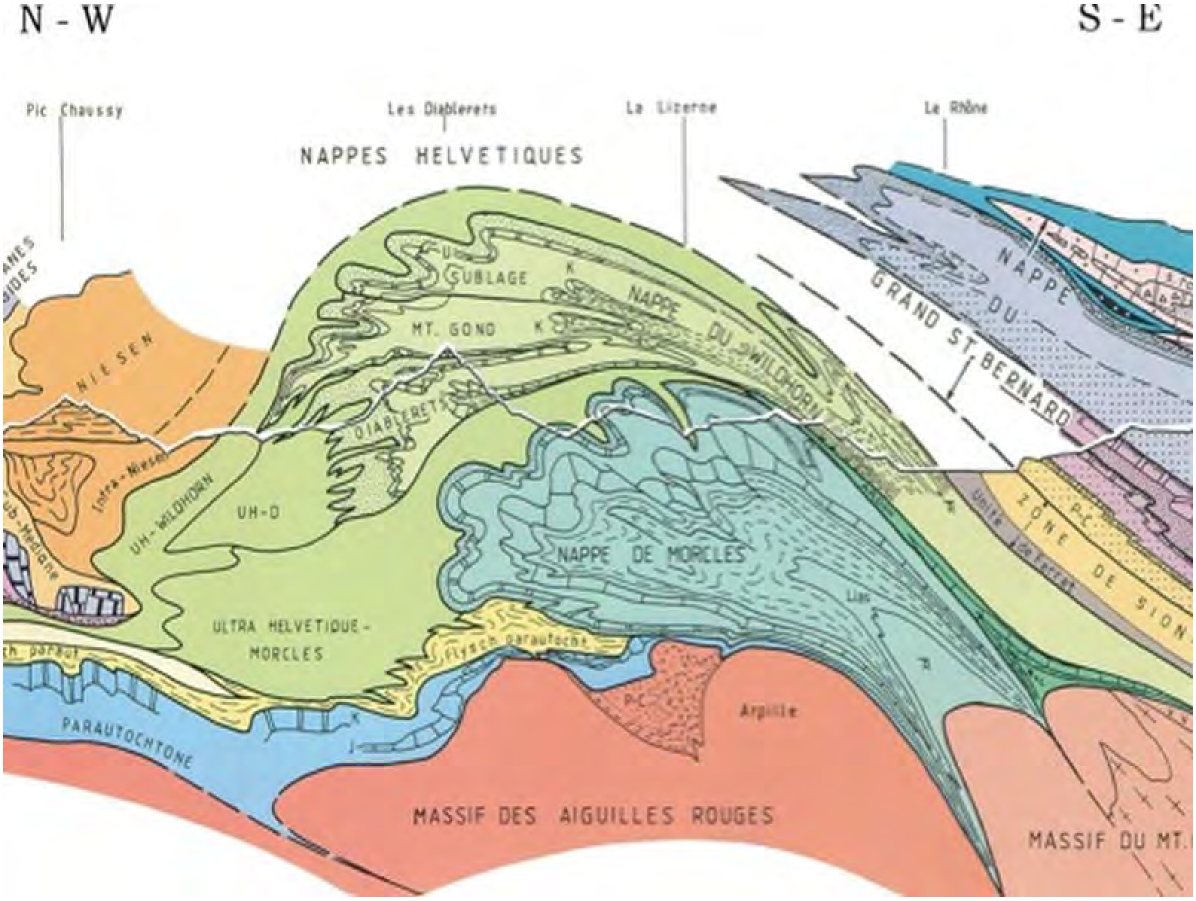

The region of Tsanfleuron is part of the Wildhorn Nappe Complex, which comprises several superposed tectonic units, including the **Diablerets** and **Mont Gond nappes**.

The Tsanfleuron plateau itself is mainly located on the Diablerets Nappe, while adjacent areas belong to the structurally higher unit of the Mont Gond nappe.

Lithostratigraphic and hydrogeological column of the Tsanfleuron–Sanetsch area (Gremaud et al, 2009)

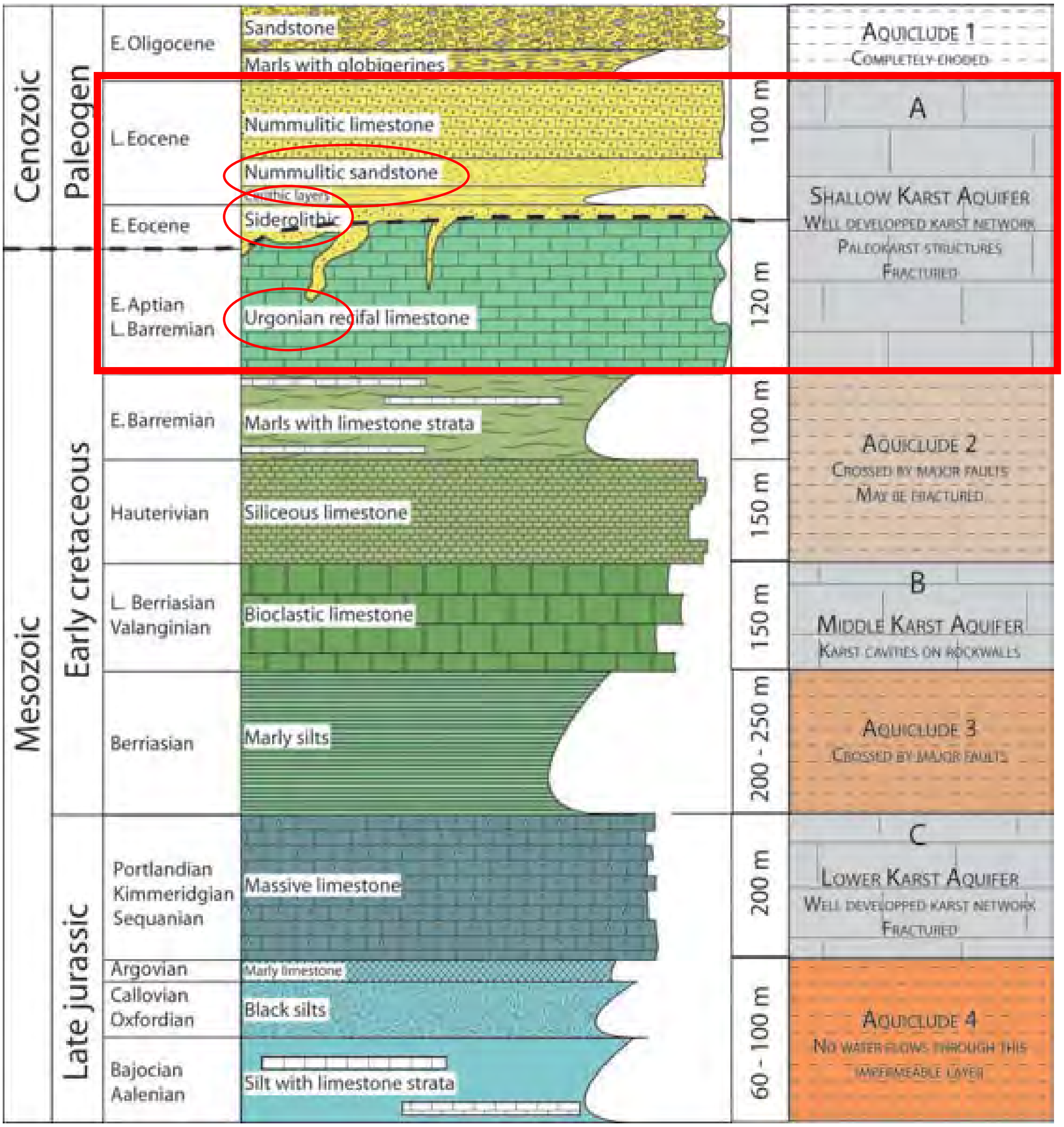

Geological map of the Tsanfleuron–Sanetsch area showing the locations of the main springs and geological cross-sections (Gremaud et al, 2009).

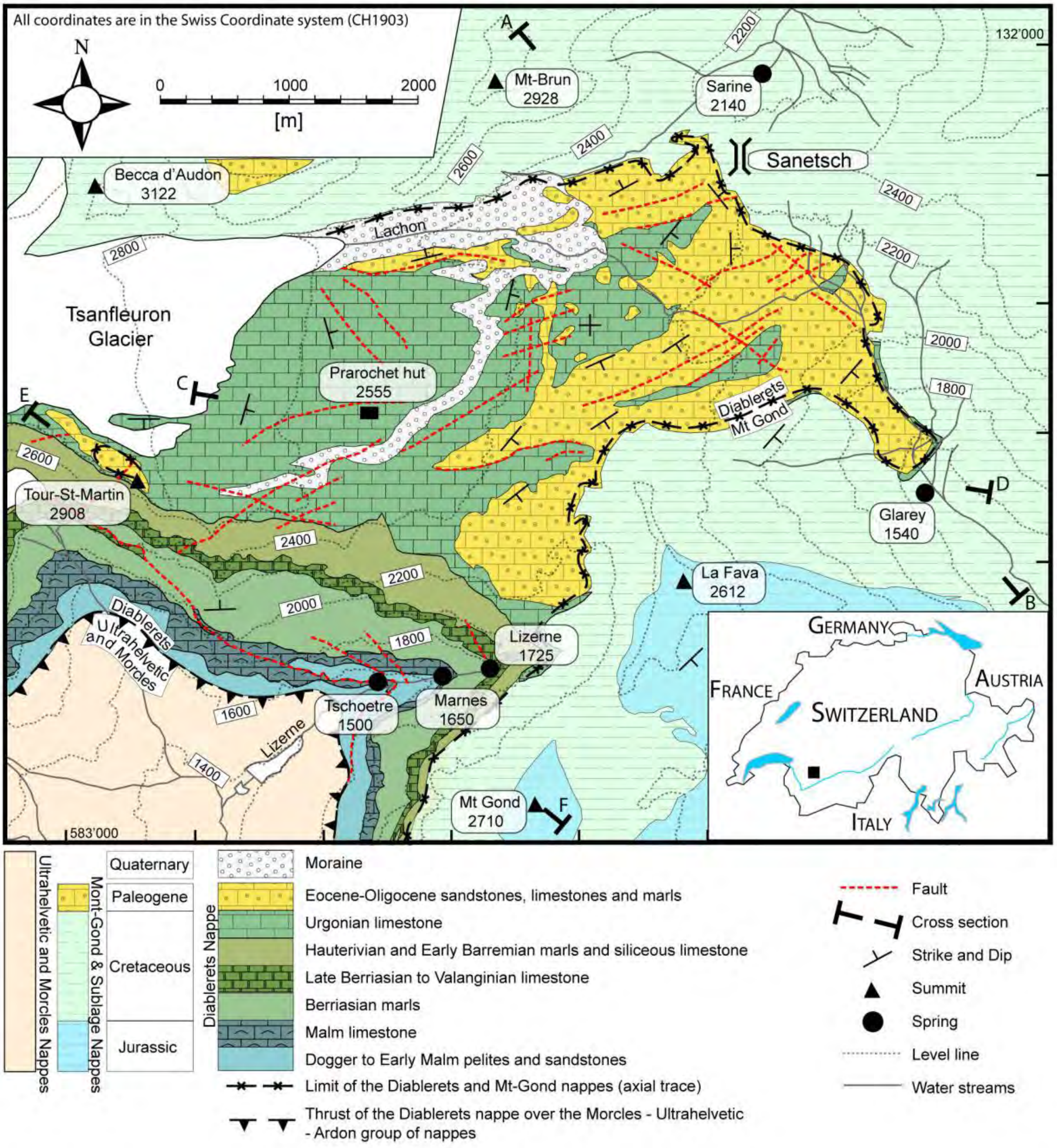

Geological cross-section from the Sanetsch Pass to the Glarey spring (see location in Figure 11). At the pass, the Urgonian limestones form a broad anticline. The Glarey spring is located within a small and tight syncline.

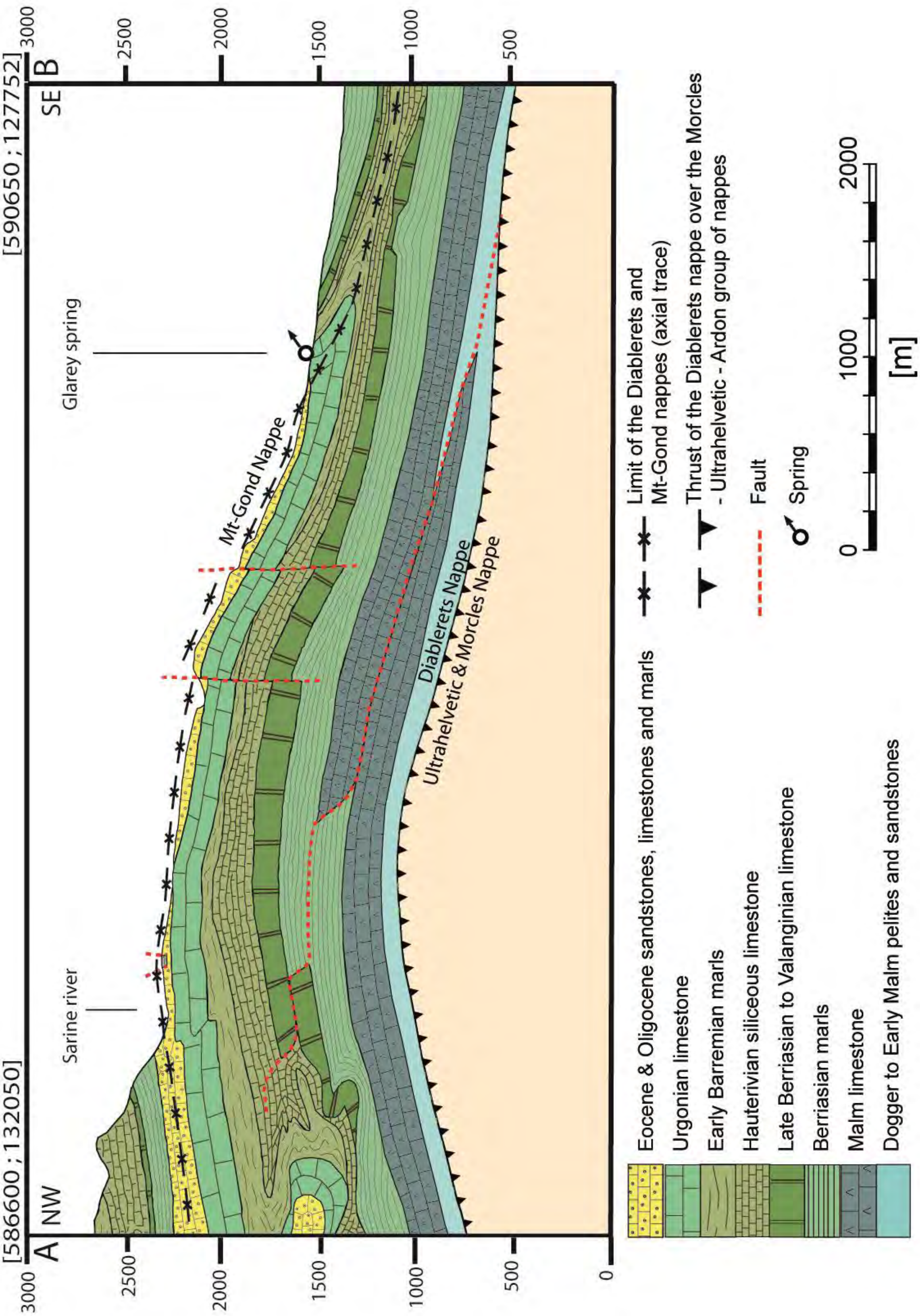

3D geological model of the Tsanfleuron area (Trottet, 2026, in progress)

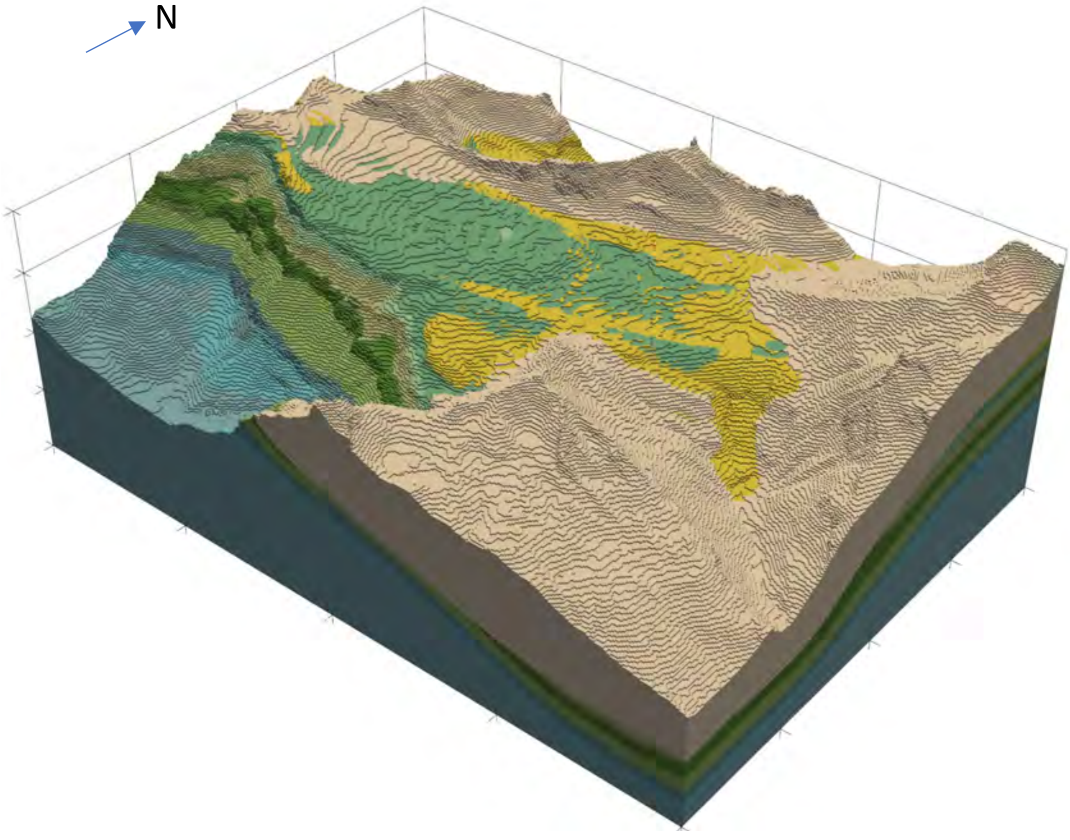

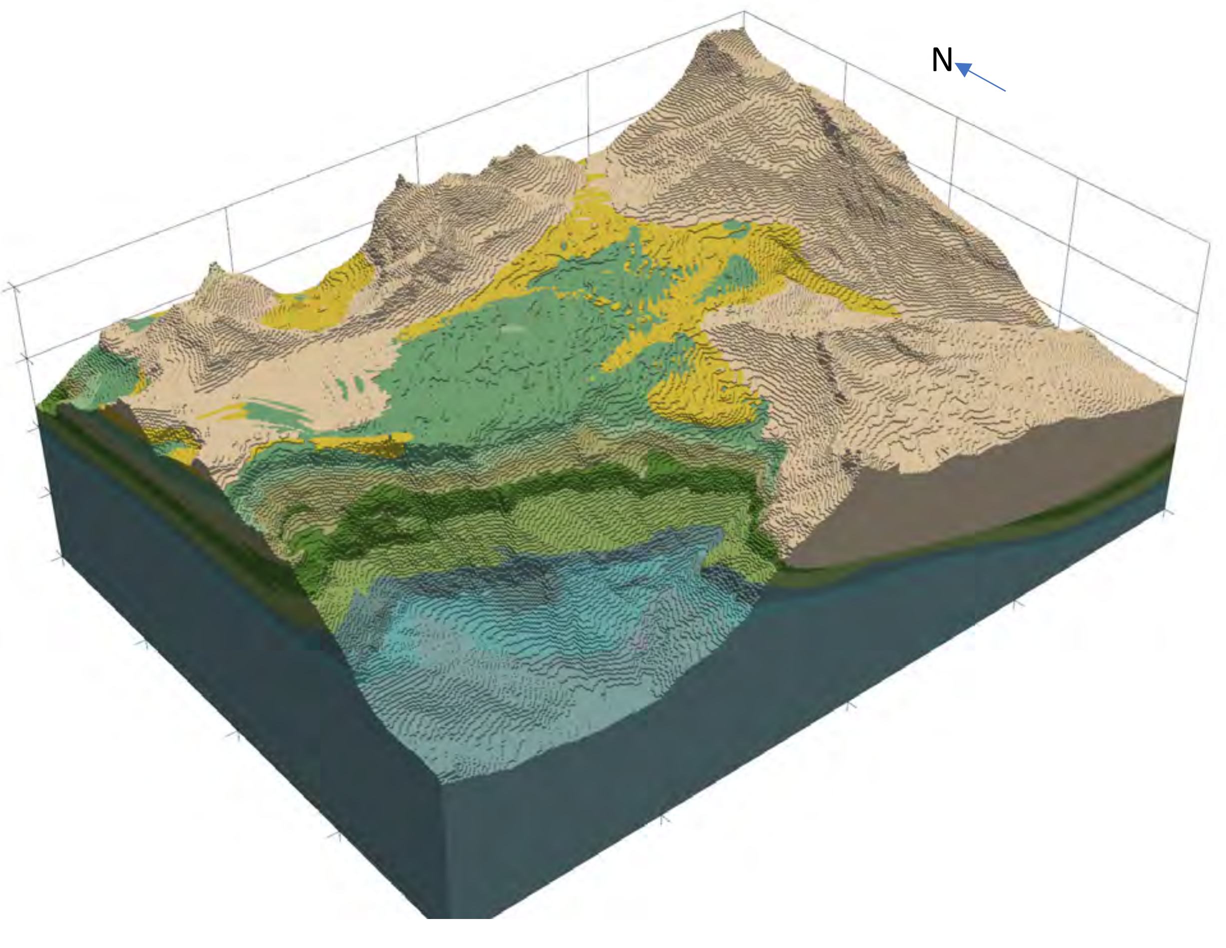

3D geological model of the area (Measday 2021).

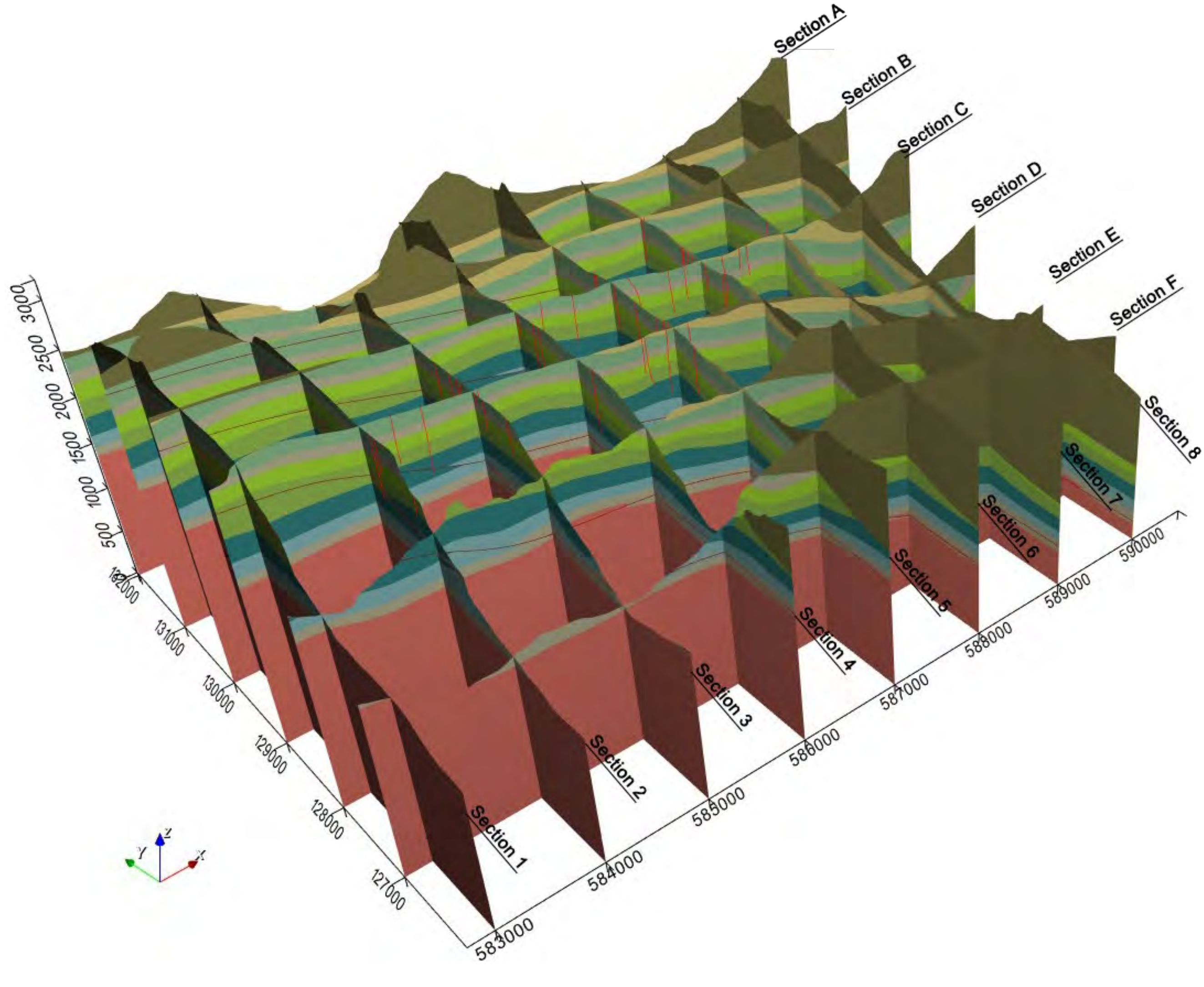

2D cross sections taken from the 3D geological model of the area (Measday 2021).

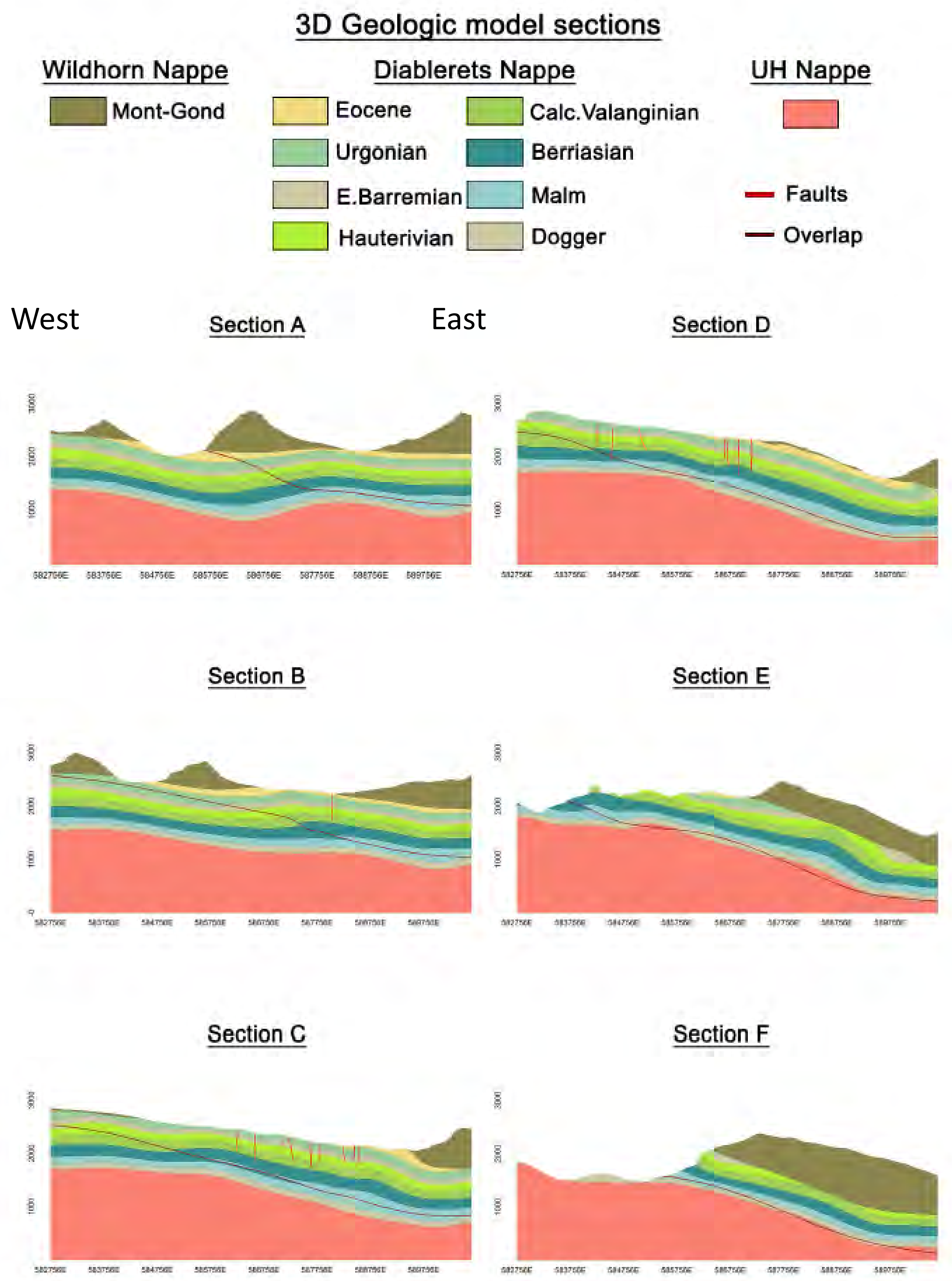

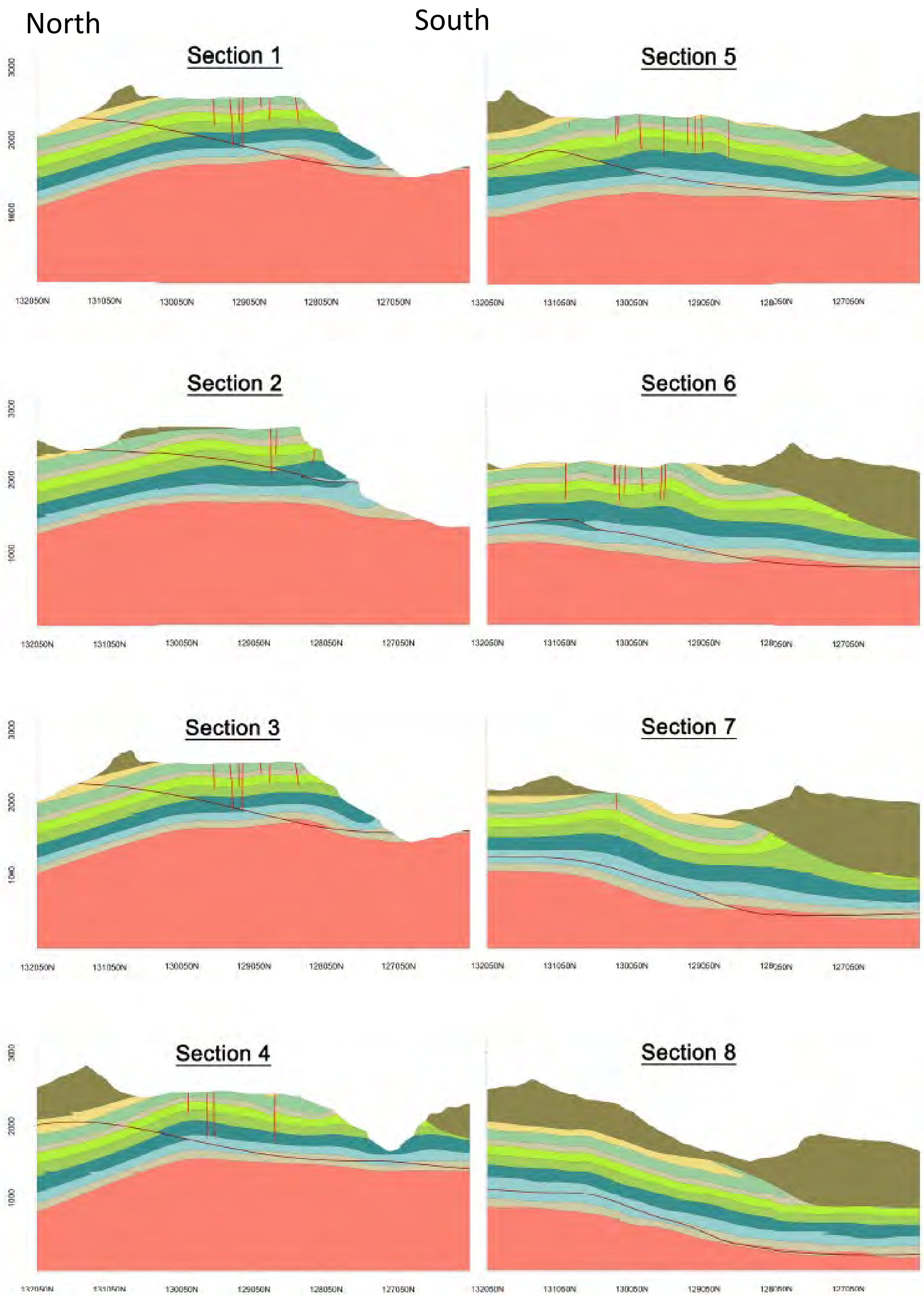

2D cross sections taken from the 3D geological model of the area (Measday 2021).

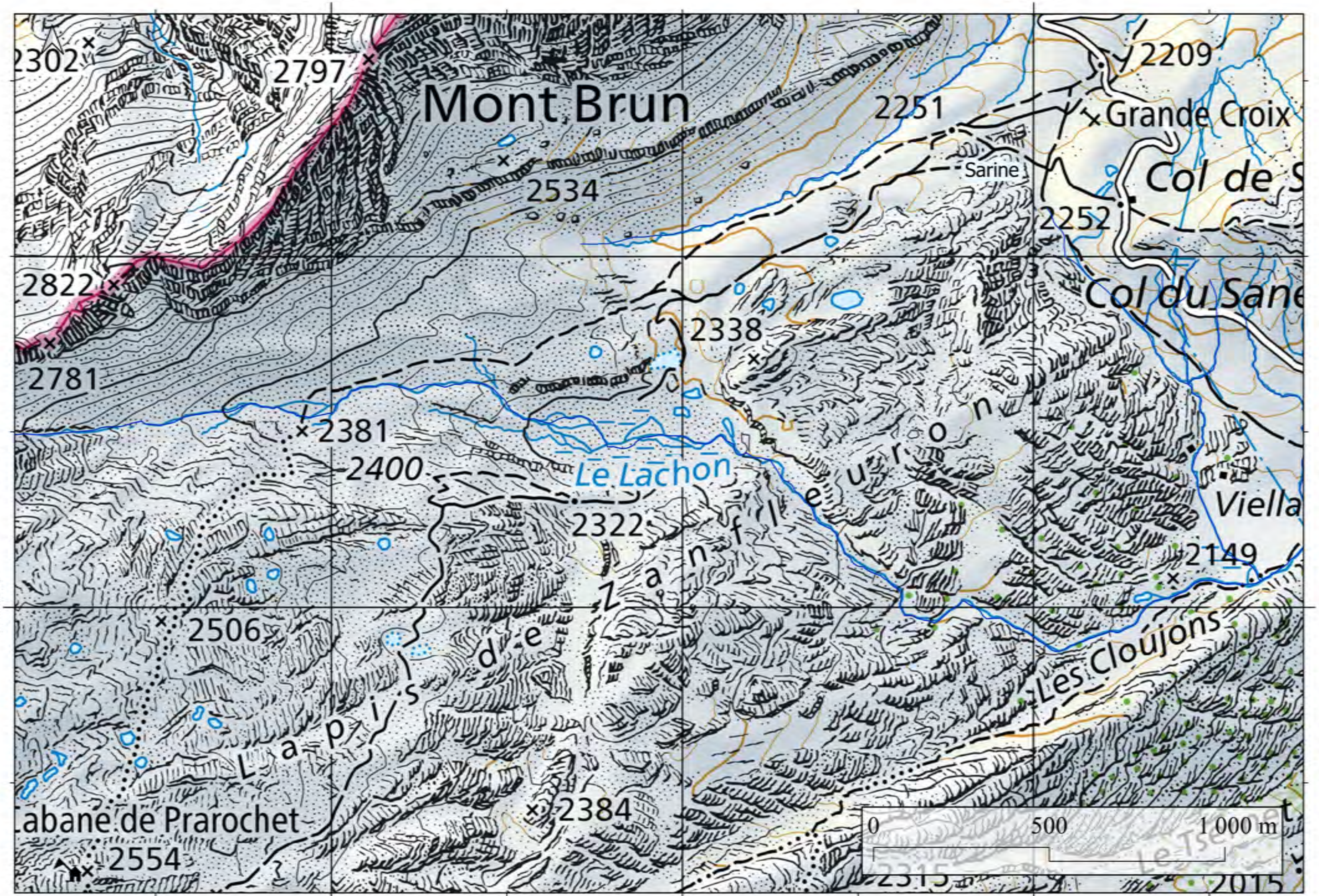
2586000
2588000
1130000
Mont Brun
2797
2302
2822
2781
2534
2251
2209
Grande Croix
Sarine
Col de S
2252
Col du Sane
2338
2381
2400
Le Lachon
2322
Lapis de Zanfleuron
Viella
2149
Les Cloujons
2506
2384
Cabane de Prarochet
2554
0
500
1000 m

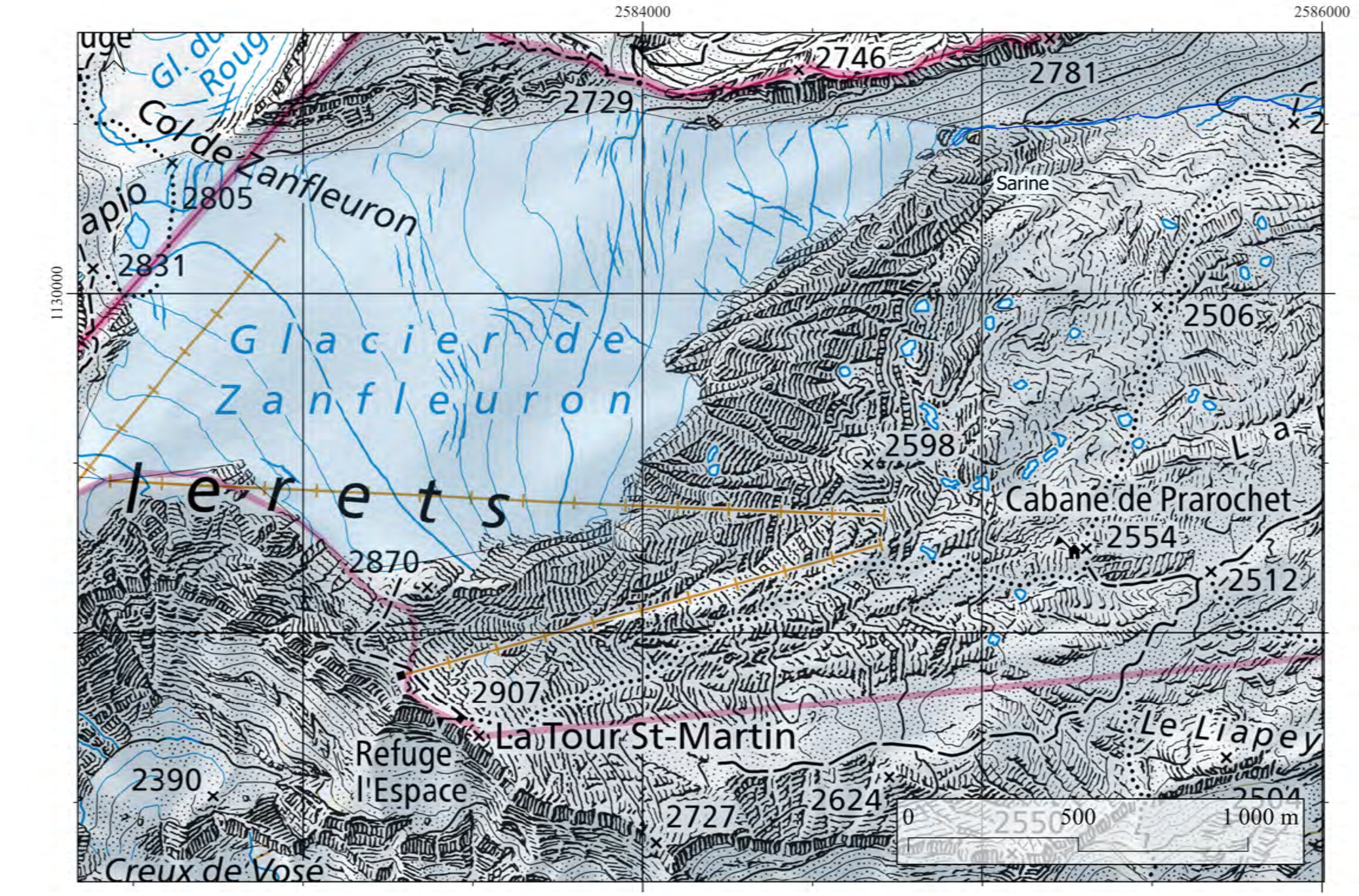

2584000
2586000
1130000
Gl. du Roug
Col de Zanfleuron
2805
2831
2729
2746
2781
Sarine
Glacier de Zanfleuron
lerets
2870
2598
2506
Cabane de Prarochet
2554
2512
2907
La Tour St-Martin
Refuge l'Espace
2390
Creux de Vosé
2727
2624
Le Liapey
0
500
1 000 m

Historical view of the glacier

Glacier view in August 2009, photo: Vivian Gremaud

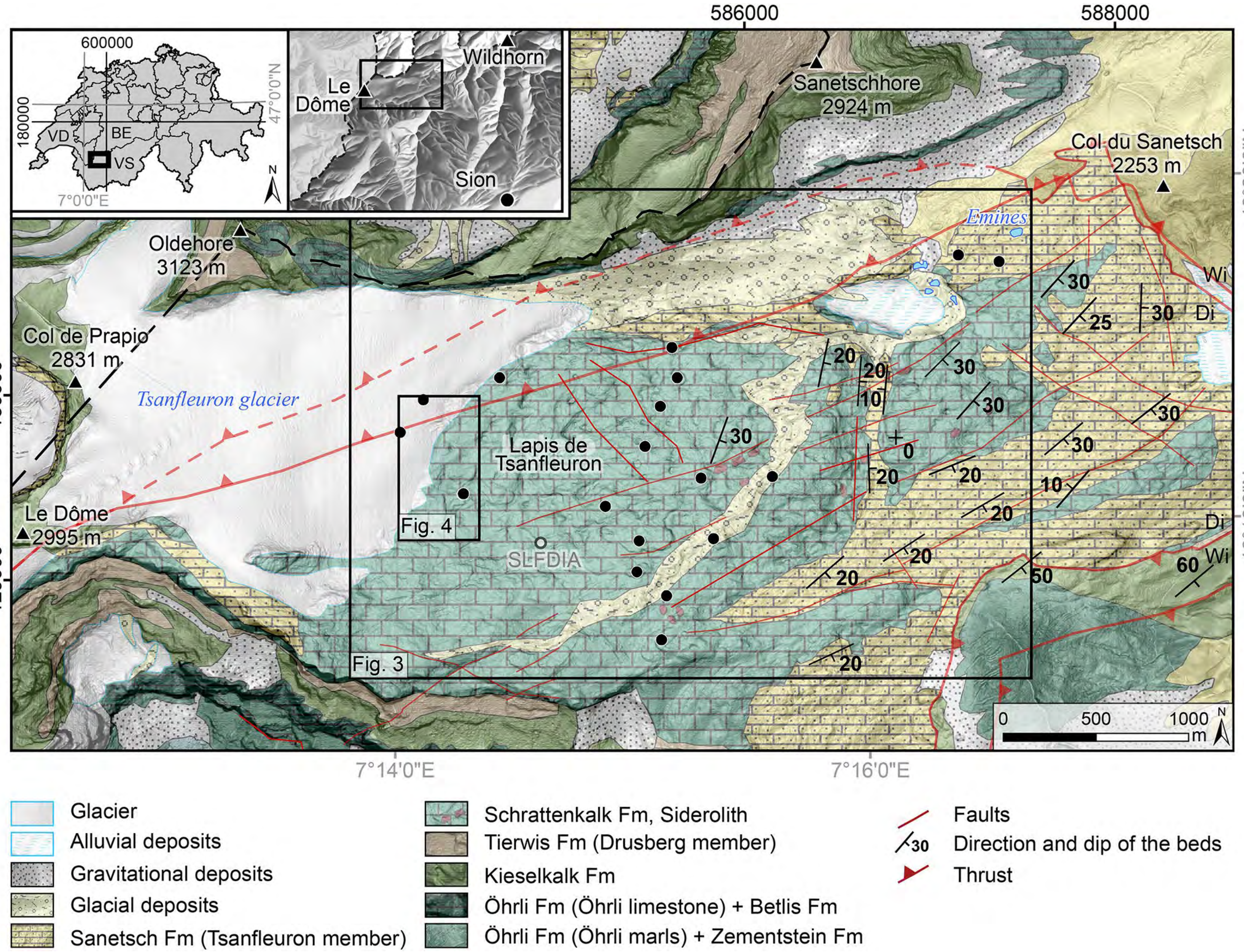

Steinemann, O., Ivy-Ochs, S., Grazioli, S., Luetscher, M., Fischer, U. H., Vockenhuber, C., & Synal, H. A. (2020). Quantifying glacial erosion on a limestone bed and the relevance for landscape development in the Alps. Earth Surface Processes and Landforms, 45(6), 1401-1417.

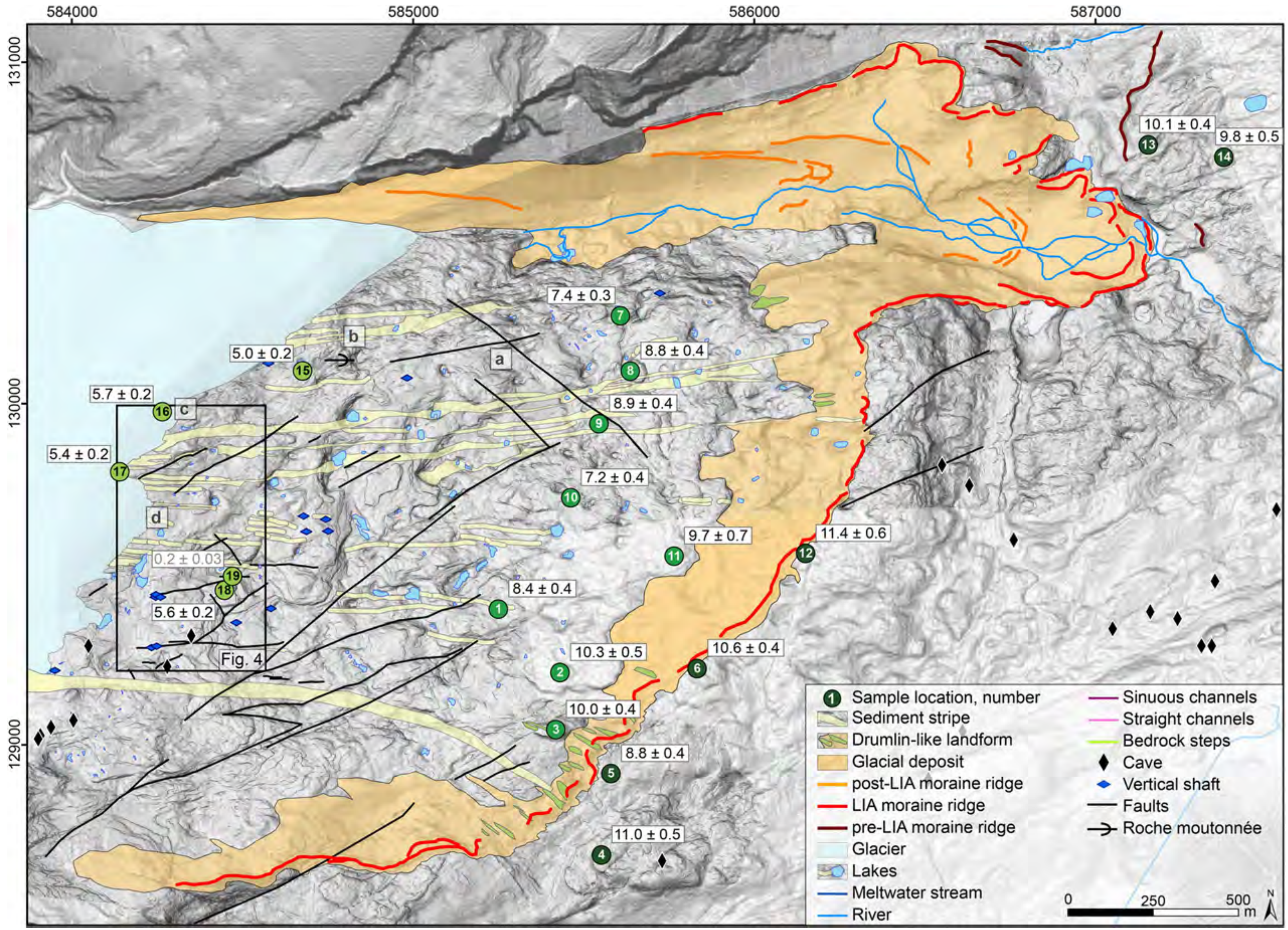

Steinemann, O., Ivy-Ochs, S., Grazioli, S., Luetscher, M., Fischer, U. H., Vockenhuber, C., & Synal, H. A. (2020). Quantifying glacial erosion on a limestone bed and the relevance for landscape development in the Alps. Earth Surface Processes and Landforms, 45(6), 1401-1417.

Lake of Emines

Between **11,400 and 10,900 cal. BP,** the presence of *Gnaphalium* seeds, unidentified deciduous leaves and moss fragments suggests an open landscape with pioneer and snow-bed vegetation.

Subsequently, **from 10,900 to 8300 cal. BP** the area around the pond was covered by alpine meadow and snow-bed vegetation as suggested by macrofossils of *Salix herbacea* and *Carex.*

Local reappearance of single trees in the mid-Holocene

Findings of 31 seeds of *P. argentea*-type after 4100 cal. BP but no findings of arboreal plant macrofossils indicate that the vegetation of Sanetsch Pass was characterised by open alpine meadows during the late-Holocene.

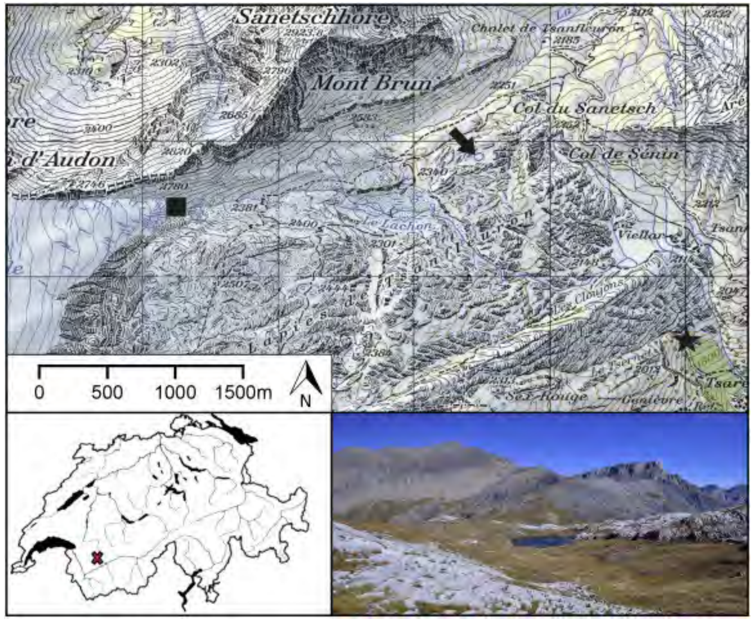

Local glaciation, (Post Würm (LGM)): local glaciers advanced in the morge valley, down to 750 m elevation. After the Late Glacial, the only extensive glaciation was that of the LIA.

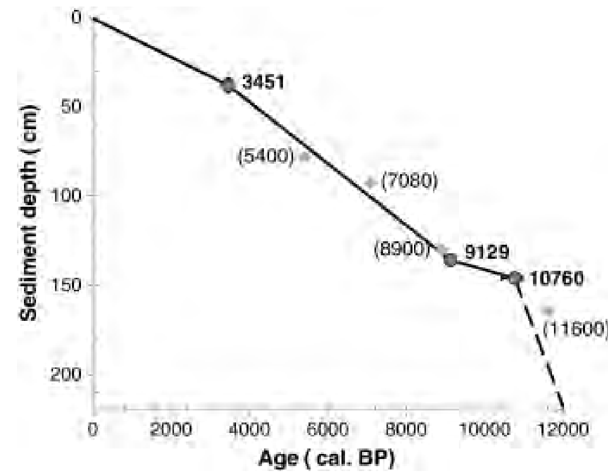

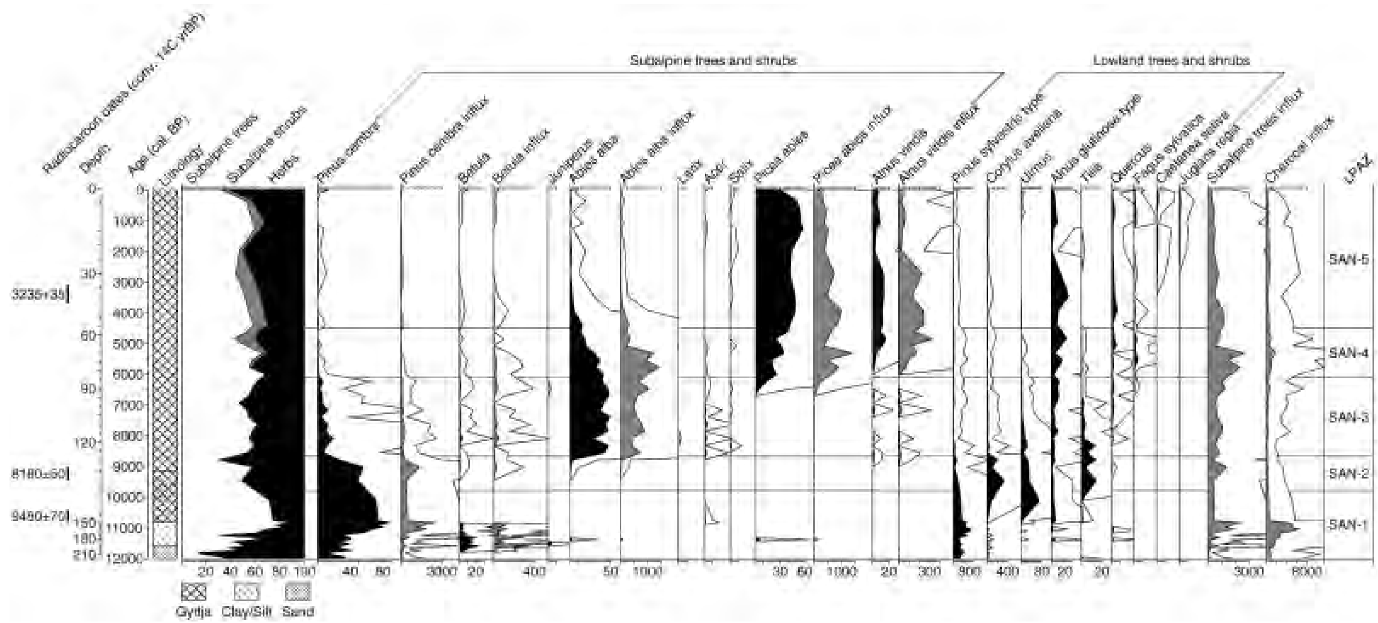

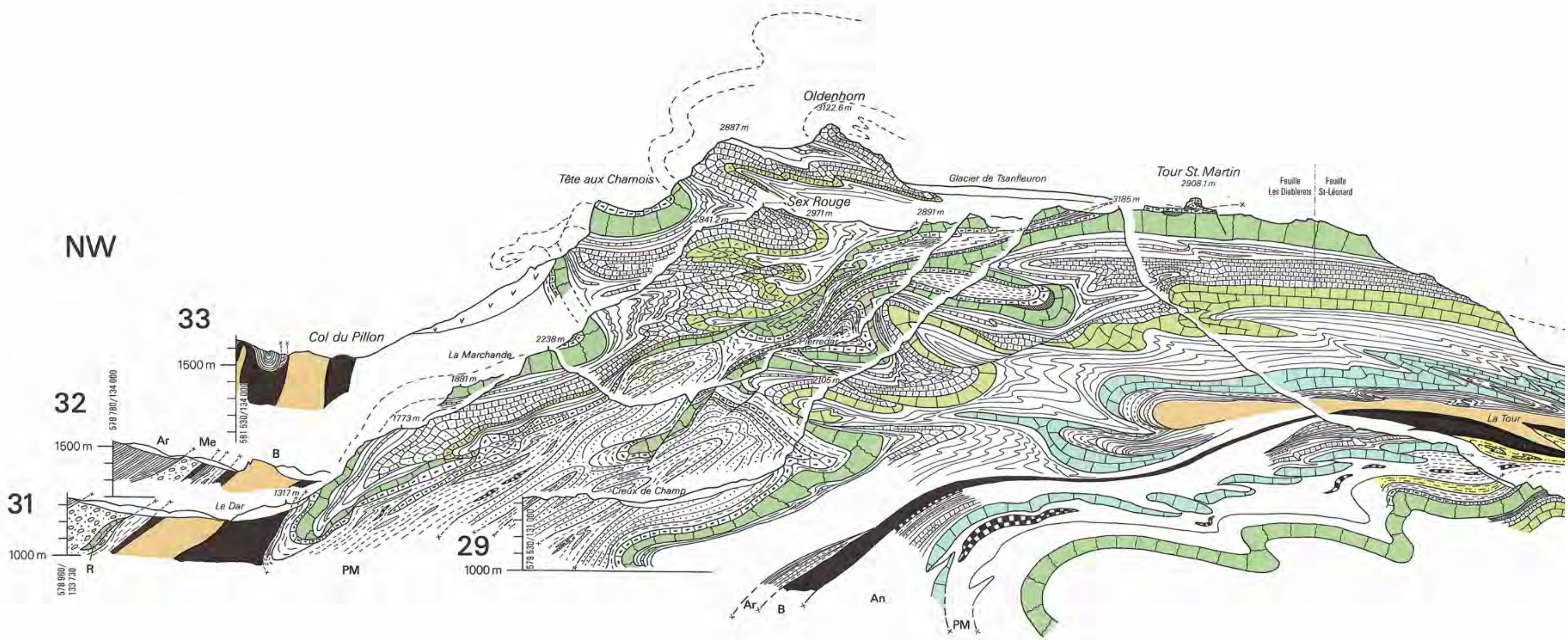

Cross-section(s) through Diablerets massif. GA25_088_Plate_II_Section_29-33 G.H. Gabus (1991)

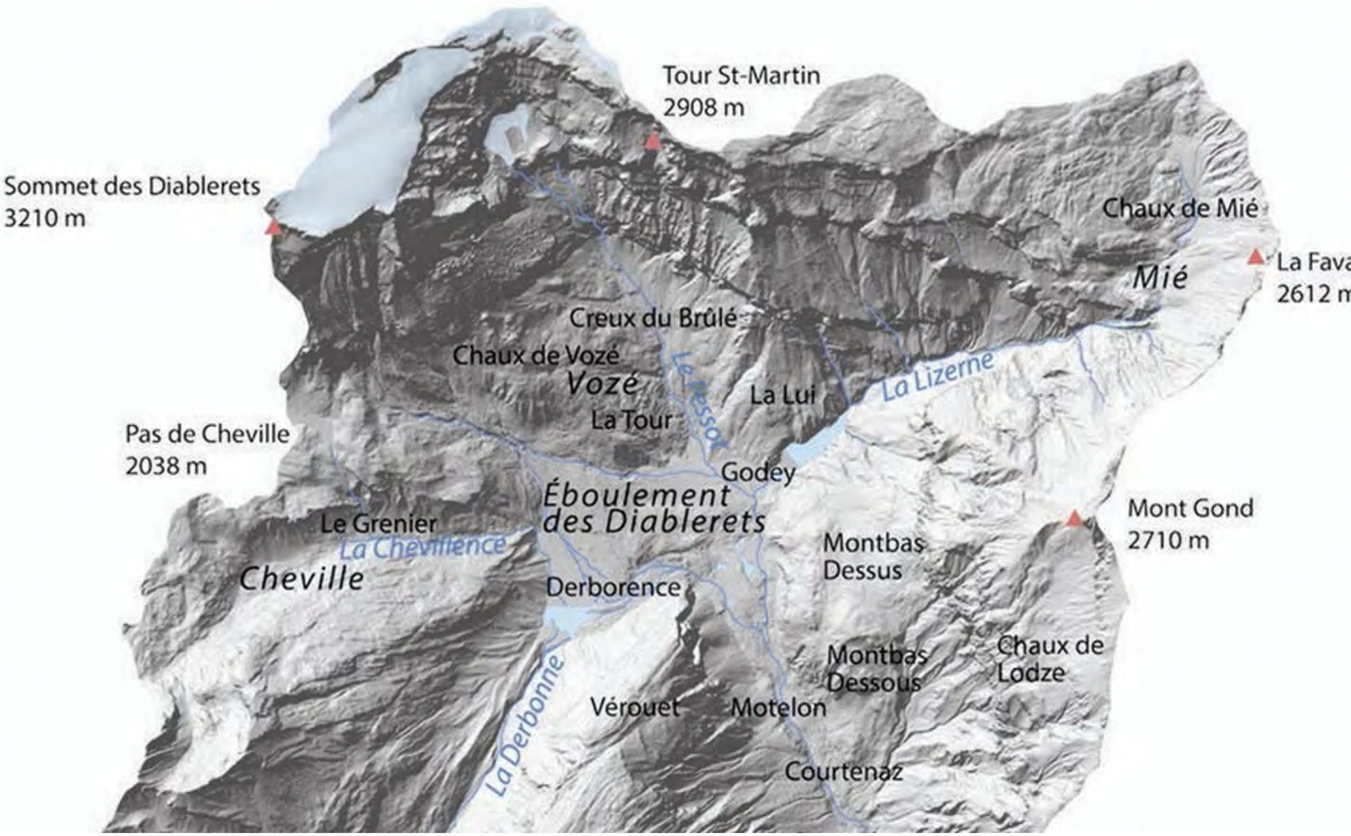

Head scarm and historical mass movement deposit incised by debris flow channel, now artificially channeised.

GARAZI, G., & A. MORET 1999. Eboulements de Derborence : Etude géologique et géomécanique (Valais / Suisse). Travail de diplôme de géologie. Section des Sciences de la Terre de l'Université de Genève.

Maret, H., & Reynard, E. (2014). Géomorphologie de la région de Derborence.

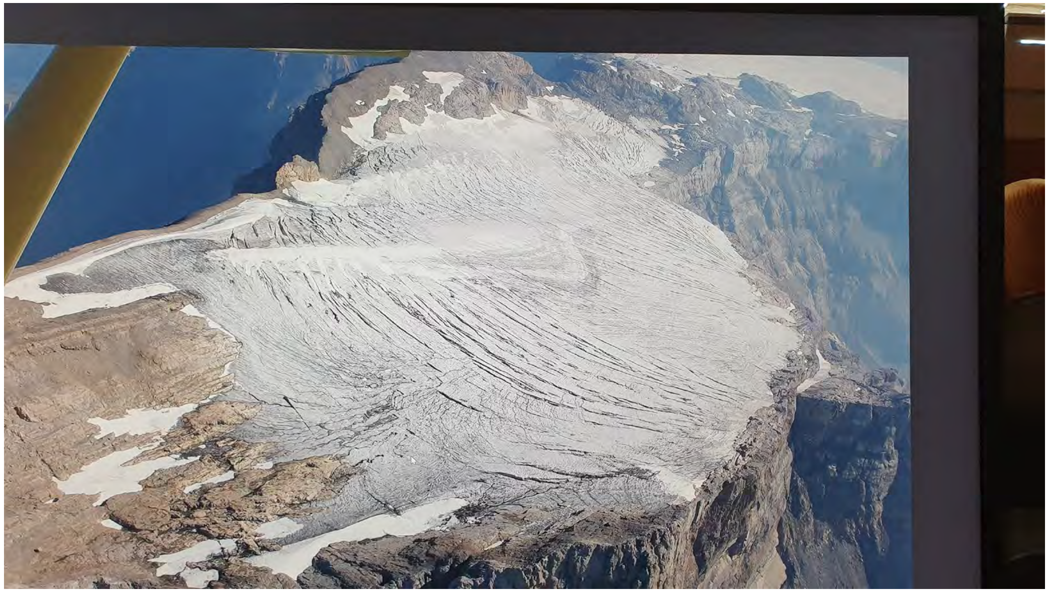

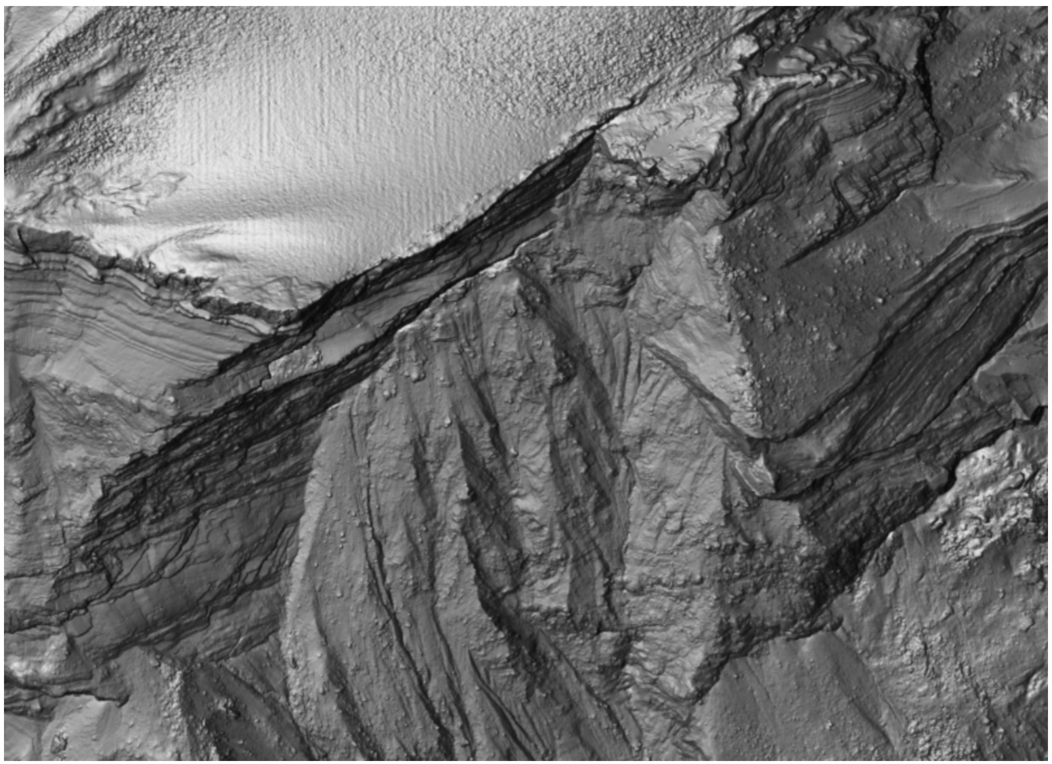

11 august 1712: earthquake felt in Vaud and Valais

23 sept. 1714 first landslide, lower part of the wall, 14 victims, along a major faultline making a weakness

1749 upper part of the wall collapses

Total volume estimated at: 45 to 67 million cubic metres, no victims. lake of Derborence appears and isolated a "virgin" forest.

1786 Phiippe Bridel, a Swiss writer and pastor narrates the chronology of events in Derboence

1934 Swiss writer Ramu writes the novel "Derborence" in French. Narrates the story of a sheperd buried alive by the 1714 event.

1961 the lake and forest of Derborence are classified and protected by Pronatura

GARAZI, G., & A. MORET 1999. Eboulements de Derborence : Etude géologique et géomécanique (Valais / Suisse). Travail de diplôme de géologie. Section des Sciences de la Terre de l'Université de Genève.

Fig. 1 Tectonic map of the Helvetic Alps of Switzerland and surrounding areas (modified from Kempf and Pfiffner 2004). Outcrop areas of the Palaeogene are highlighted in *Red*. For convenience the Swiss National Grid system is applied

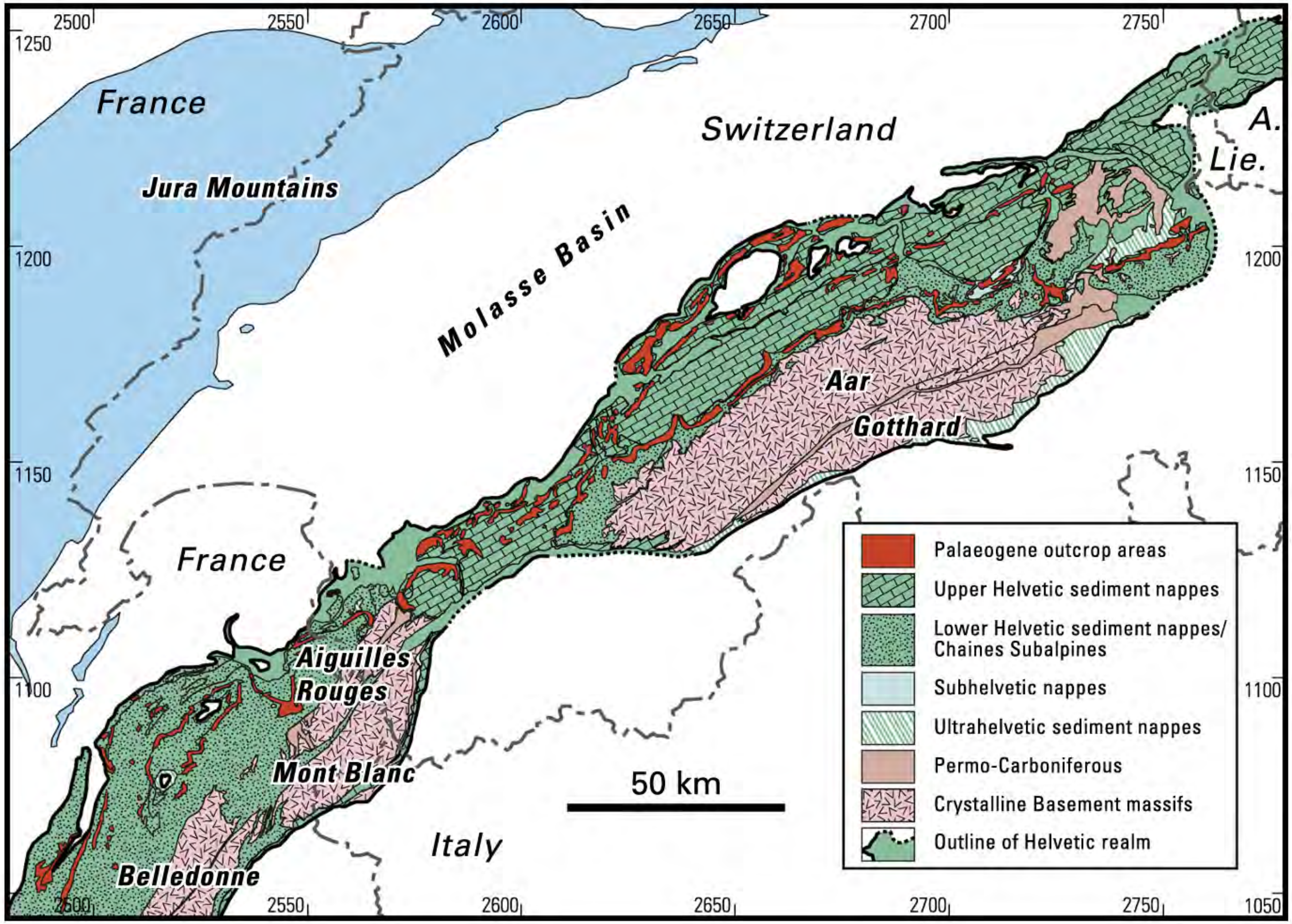

Menkveld-Gfeller, U., Kempf, O., & Funk, H. (2016). Lithostratigraphic units of the Helvetic Palaeogene: Review, new definition, new classification. Swiss Journal of Geosciences, 109(2), 171-199.

Siderolithic
Herb (1988) defined the Helvetic ''Siderolithikum'' collectively as rock unit that comprises **iron-containing, argillaceous and sandy rocks, often brecciated**, often also as ''Bohnerzton'', a pisolitic iron ore clay (with vadose pisoliths).

Key components: **Kaolinite, Goethite, Montmorillonite**

However, the rock unit does not occur merely in form of infiltrates and pockets in the underlying rocks, partially disaggregating the underlying rocks into brecciated formations. But it can also form massive beds between the underlying rocks and younger transgressive rocks above (Wieland 1976).
Description: sandstone and claystone,matrix of a breccia. Presence of elongate, mostly black pisoliths composed of hematite and chamosite. Siderolithic breccia and conglomerate beds can be locally up to 50 m thick. **The siderolithic rocks are an unequivocal indicator of terrestrial conditions.**

Found in deep-reaching karst pockets and caves is characteristic of regions with siderolithic formations. These can extend as much as 100 m below the base of the Palaeogene and are often bound to preexisting networks of fissures: indicators of significant uplift and emersion.

Concerning the age, the rocks of the Siderolithic Group must have formed prior to the Priabonian; that is, before the deposition of the Niederhorn and Sanetsch Formation
Some rodent tooth dating suggest Bartonian approx. 40-37 Ma (just before Priabonian age 37-35 Ma)

Menkveld-Gfeller, U., Kempf, O., & Funk, H. (2016). Lithostratigraphic units of the Helvetic Palaeogene: Review, new definition, new classification. Swiss Journal of Geosciences, 109(2), 171-199.

In-cave monitoring

- adapted water sampler for natural tracers, incl. stable isotopes (Michelsen et al., 2019)
- use of weir for a shallow cave stream flow rate
- temperature and conductivity to single out snow melt / rain events

Figure: cave weir and sampler

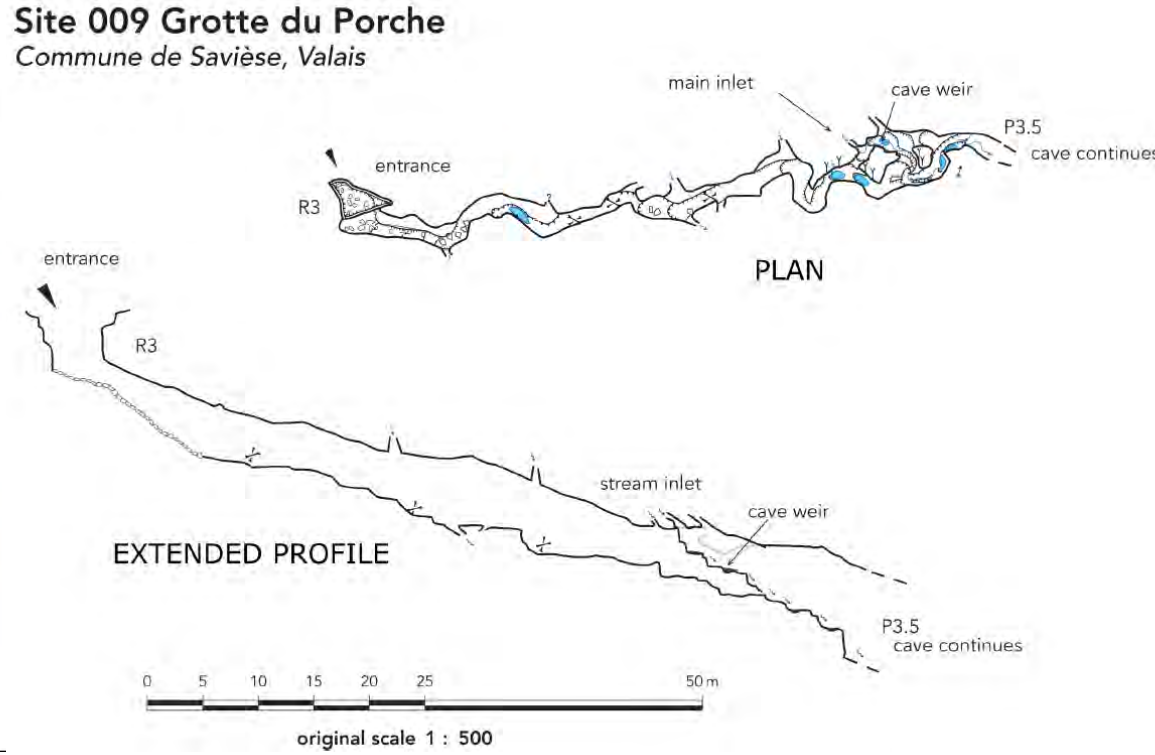

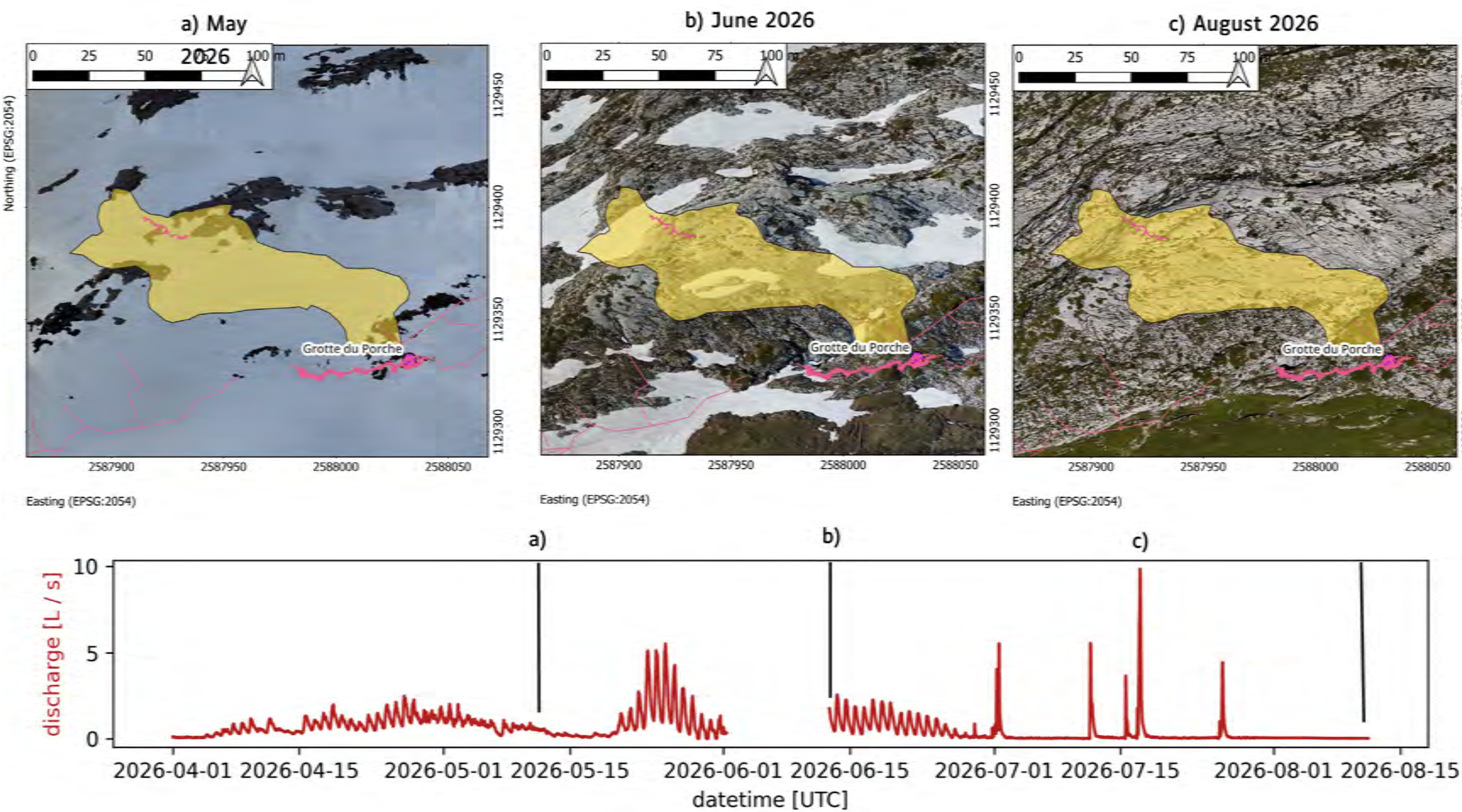
a) May 2026
b) June 2026
c) August 2026
0 25 50 75 100 m
Grotte du Porche
Northing (EPSG:2054)
1129450
1129400
1129350
1129300
2587900
2587950
2588000
2588050
Easting (EPSG:2054)
a)
b)
c)
discharge [L / s]
0
5
10
2026-04-01
2026-04-15
2026-05-01
2026-05-15
2026-06-01
2026-06-15
2026-07-01
2026-07-15
2026-08-01
2026-08-15
datetime [UTC]

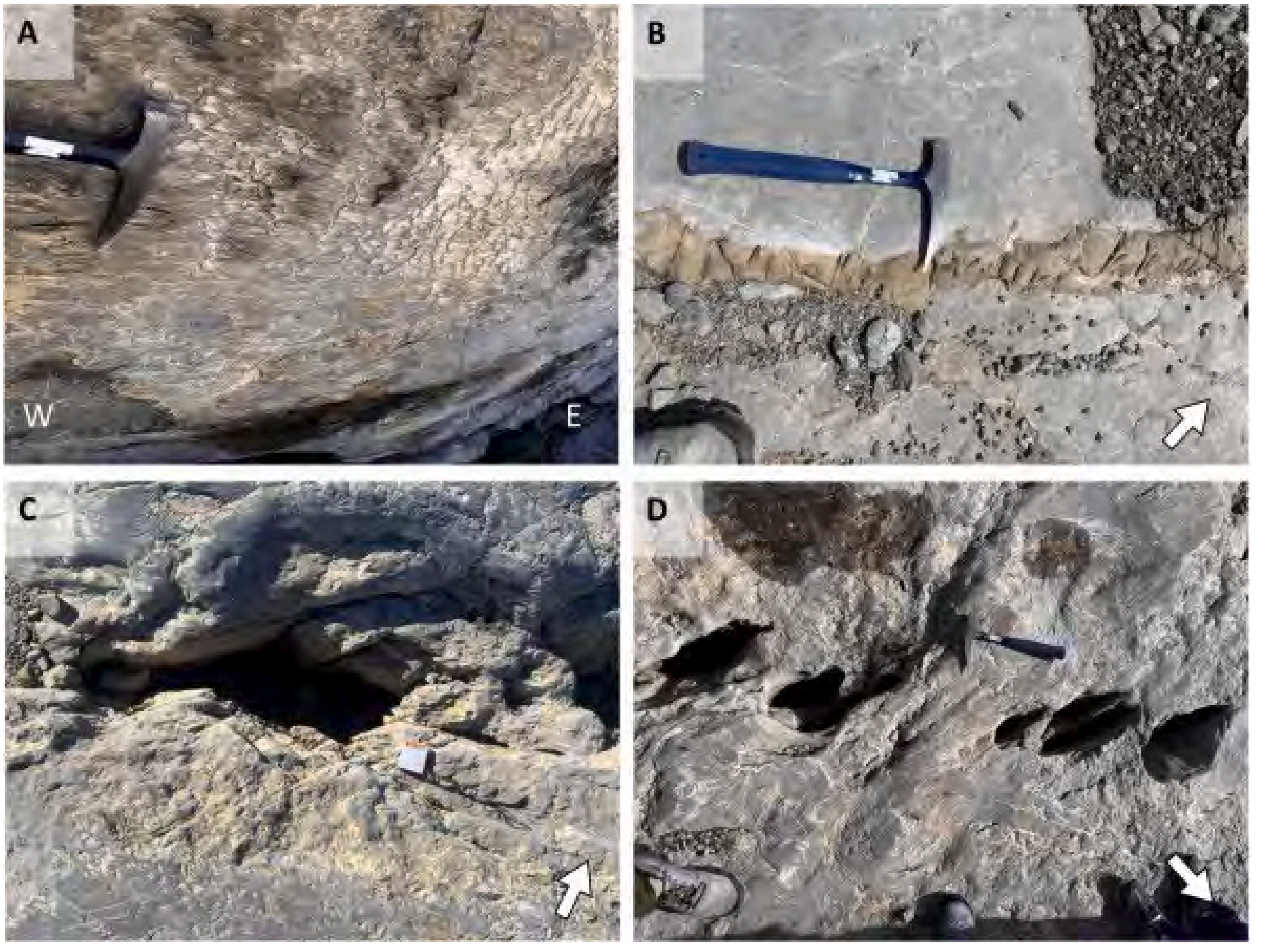

Details of the structural and dissolution features: (A) slickenside indicating lateral movement (dextral), (B) NE-SW fracture filled with siderolitic deposits, (C) rhombohedric dissolution, (D) NW-SE fractures with en echelon dissolution.

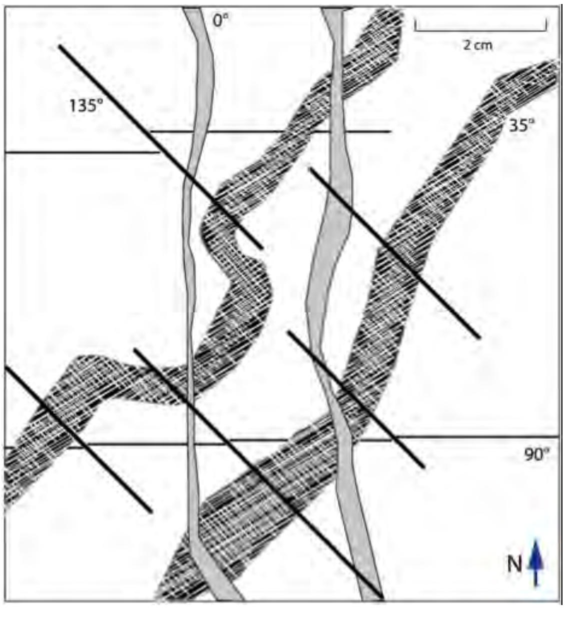

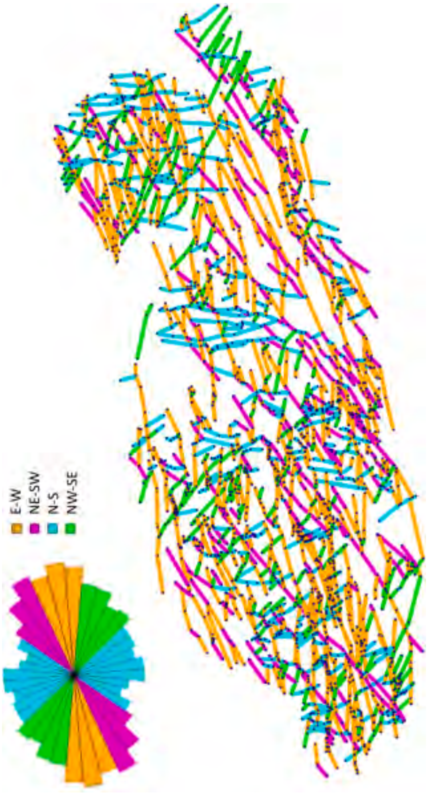

Tanaka, A. P. B., Renard, P., de Moraes Caldeira, J. N., & Trunz, C. (2025). Graph-based fracture network analysis to integrate structural geology properties and identify preferential flow pathways in the aquifer system of Tsanfleuron, Swiss Alps. *Journal of Structural Geology*, 105543.

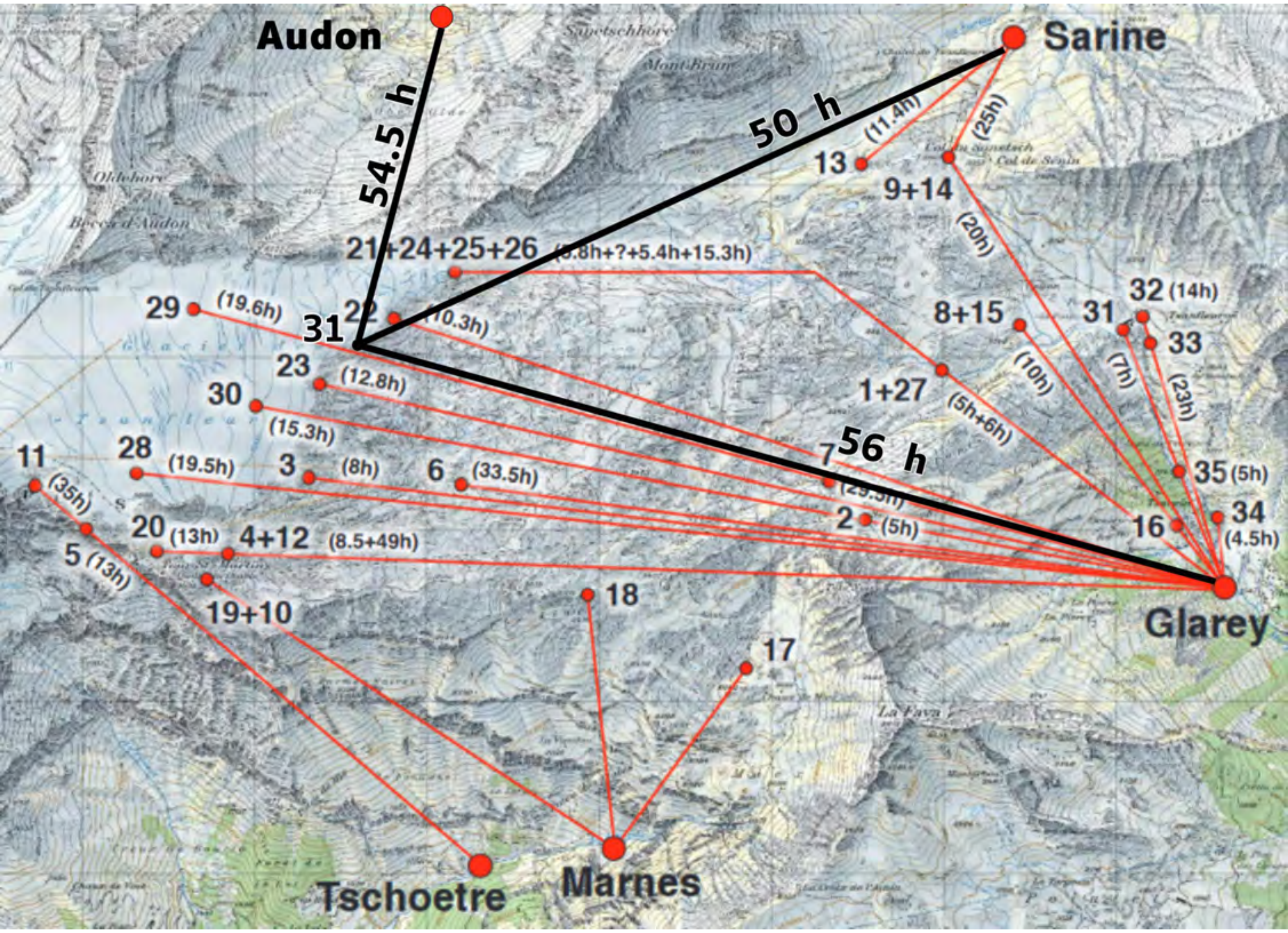
Audon
Sarine
54.5 h
50 h
56 h
13
(11.4h)
(25h)
9+14
(20h)
21+24+25+26
29
(19.6h)
31
22
(10.3h)
23
(12.8h)
30
(15.3h)
11
(35h)
28
(19.5h)
3
(8h)
6
(33.5h)
20
(13h)
4+12
(8.5+49h)
5
(13h)
19+10
18
17
8+15
(10h)
1+27
(5h+6h)
7
2
(5h)
32
(14h)
31
(7h)
33
(23h)
35
(5h)
16
34
(4.5h)
Glarey
Tschoetre
Marnes

- **Diablerets member**: type section- 2586720 1129395
- The Diablerets Member is built only locally as a filling of a palaeorelief at the top of Cretaceous deposits and reflects the onset of a transgression.
- The member was presumably deposited over a large area, but eroded again to a great extent (except for pockets and depressions) when the full marine transgression commenced.
- During the transgression the underlying Cretaceous formations were reworked and breccia or conglomerate beds were deposited with a local spectrum of pebbles.

- **Tsanfleuron Member**
- The base of the Tsanfleuron Member is commonly built as quartz sandstone to calcareous sand stone devoid of fossils, often with bimodal grain-size distribution.
- Frequently it fills karst fissures in the top of the underlying Cretaceous strata. Sediments of the transition to the inner shelf, sandstone to micrite, follow with the first Corallinaceans.
- The sand supply decreases upsection, a sandstone bed or a sandy limestone bed terminates the member towards the top.
- The Tsanfleuron Member is preserved discontinuously, laterally it can be represented by a conglomerate bed with a sandy matrix, by a sandstone bed with plenty of large oysters, or it can be missing. The thickness is up to 17 m.

- **Pierredar Kalk**
- Pierredar-Kalk (Pierredar Limestone) represents the Sanetsch Formation in part as the sole stratigraphic member.
- This manifold limestone is characterised by abrupt vertical and horizontal facies changes and was deposited on a carbonate platform. Corals occur only secondarily and at few locations.
- Micrite, mainly built of Corallinaceans with local clusters of benthic Larger foraminifera, and marly micritic limestone with Discocyclines and many clasts of benthic Lithostratigraphic units of the Helvetic Palaeogene: review, new definition, new classification 187 Larger foraminifera are predominant lithologies.
- Often the Discocyclines-rich limestone overlays the Corallinacean limestone (‘‘Lithothaminen-Kalk’’),whichformed insome what shallower water under calm conditions.
- A transition of the Pierredar Limestone into the marl of the Stad Formation as a result of increasing marl content is rare. Most often the boundary is distinct, although a change in the depositional area is signalised by the appearance of planktonic foraminifera.

Subglacial calcite crusts

Sparite (Figures 2aand3a) is milky white in color and consists of pure calcite crystals up to 1 mm in diameter and 2 cm long. Crystals have an acicular form and are elongated parallel to the direction of ice flow as indicated by bedrock striations. The occurrence of sparite is patchy, individual outcrops having an area of only a few square centimeters and a thickness of a few millimeters.
X-ray diffraction analysis reveals the presence of calcite alone, and the acid insoluble residue content is always less than 10%.

Micrite is light brown to beige in color in surface out-crop, but appears grayish when seen in section. It is more abundant than sparite, occurring as surface crusts up to 10 mm thick, which cover areas as great as 0.5 m. The upper surface of these crusts consists of ridges and furrows aligned parallel with the ice flow direc-tion.
Individual calcite crystals are usually less than 10JLmin size. Micrite consists of calcite which contains consider-able amounts of impurities (mean acid insoluble residuecontentof16%) ,including particlesofquartz(10-100JLm), muscovite (5-50JLm),lithic frag-ments«1500JLm),hematite nodules (5-60JLm),finelydividedpyrite,illite,andchlorite,andlarger calcitecrystals

Maire, R. (1990). La haute montagne calcaire(karsts. Cavités. Remplissage. Quaternaire. Paléoclimats). *Karstologia-Mémoire*.

Sharp, M., Tison, J. L., & Fierens, G. (1990). Geochemistry of subglacial calcites: implications for the hydrology of the basal water film. *Arctic and Alpine research*, *22*(2), 141-152.

Estimation of glacier ice thickness in 2018 using ground-penetrating radar (GPR). Instruments, data acquisition on the glacier, and example of raw data (signal intensity as a function of travel time) – Bachelor's thesis by Marie Vallat and Cyprien Louis.

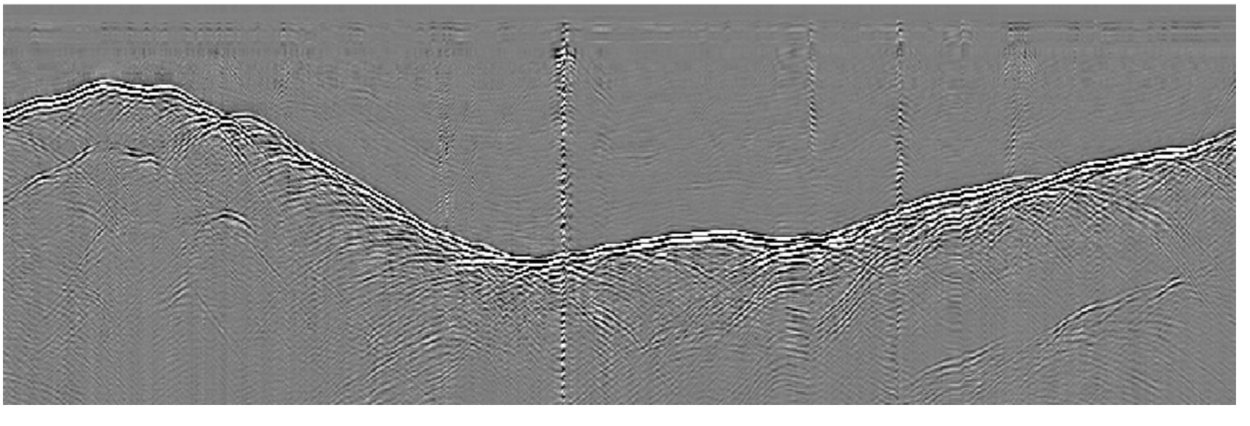

GPR data points – along walking tracks (Vallat, 2020).

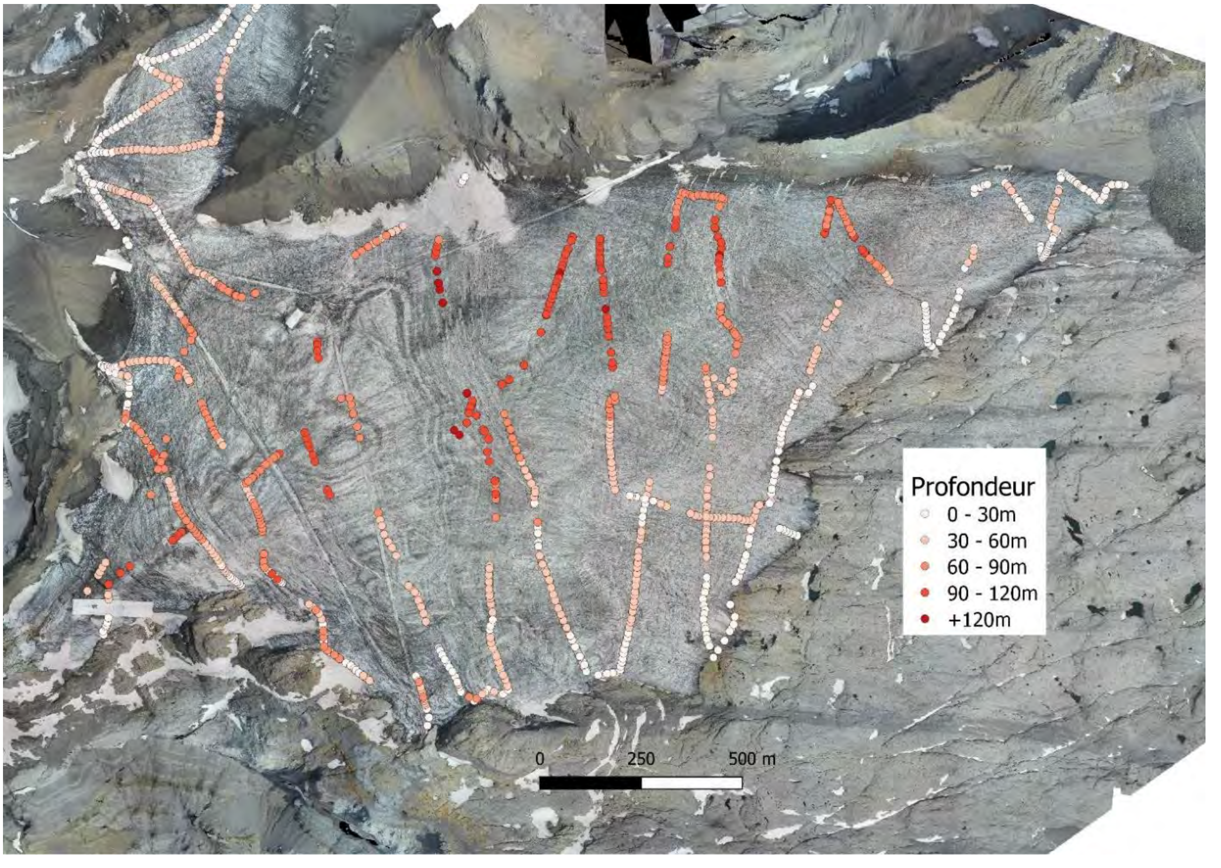

Photogrametry DEM E-Bee Sensefly drone data from 2019, (Louis, 2020)

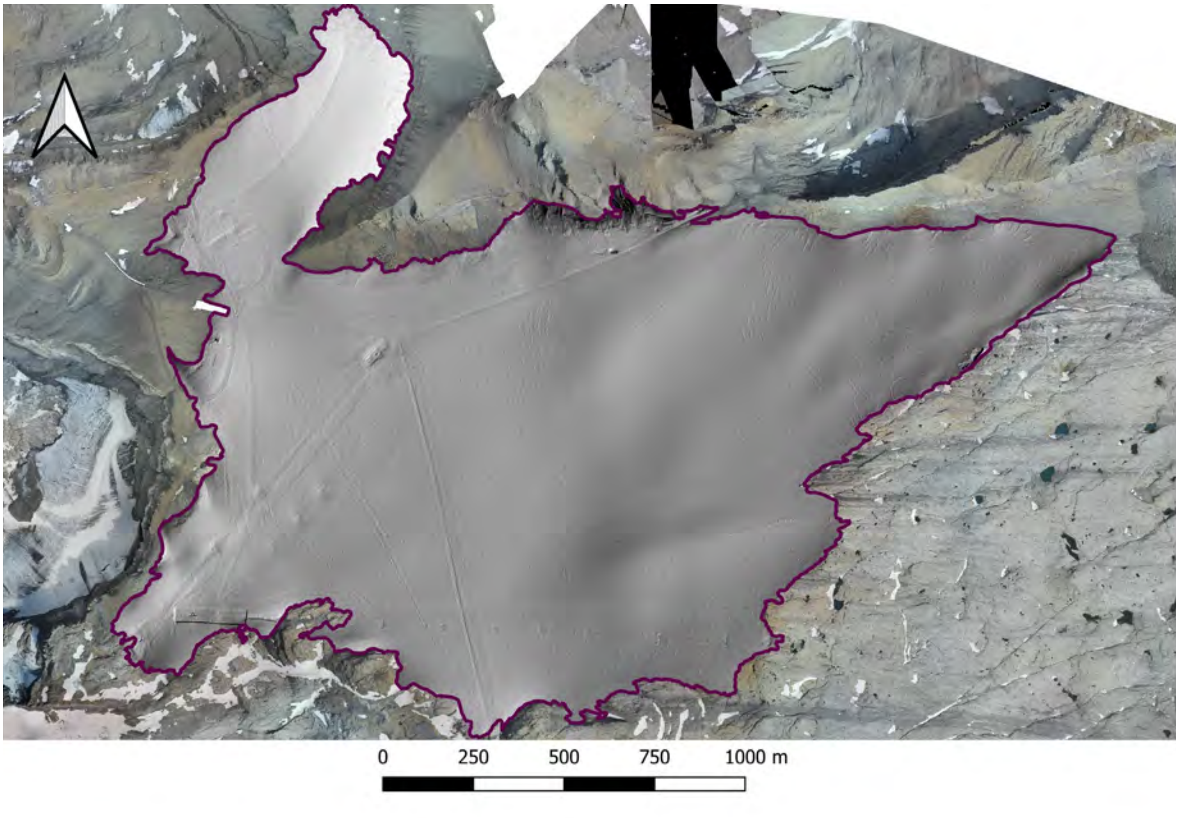

Estimated ice thickness (Neven et al., 2021)

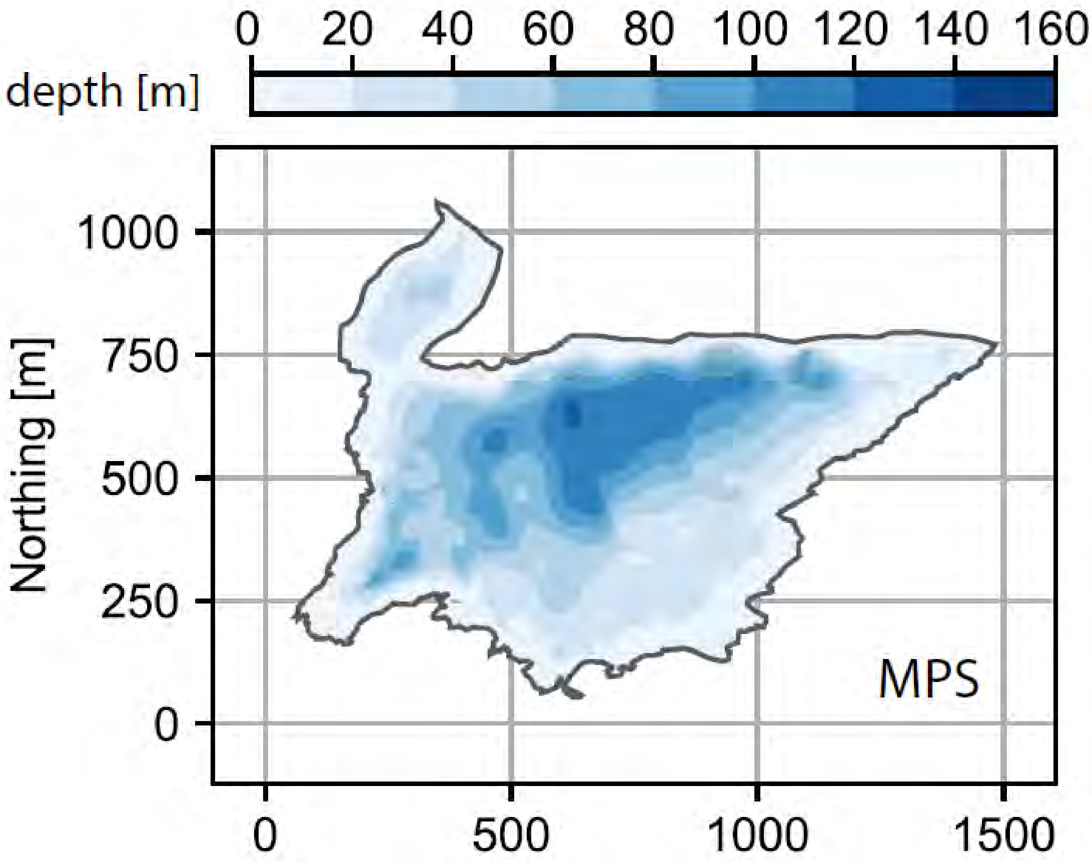

Method	Tsanfleuron 2019 [$mio\ m^3$]	Tsanfleuron 2011 [$mio\ m^3$]	Scex-Rouge 2019 [$mio\ m^3$]	Scex-Rouge 2011 [$mio\ m^3$]	Total 2019 [$mio\ m^3$]	Total 2011 [$mio\ m^3$]
MPS	109.8 ± 1.5	143.2 ± 1.5	4.1 ± 0.3	6.6 ± 0.4	113.9 ± 1.6	149.8 ± 1.6
SGS	109.7 ± 1.7	143.3 ± 1.8	4.2 ± 0.2	7.05 ± 0.2	113.9 ± 1.8	150.4 ± 1.8
Kriging	109.0	143.0	4.1	6.8	113.1	149.9

Estimated evolution of ice volume. Gremaud & Goldscheider (2010) estimated an annual ice loss of approximately **4.2 million m³ per year**. At this rate, the glacier was projected to disappear completely by **2035**. Based on new ground-penetrating radar (GPR) data, Louis (2020) revised this estimate and projected the glacier's disappearance **beyond 2040**.

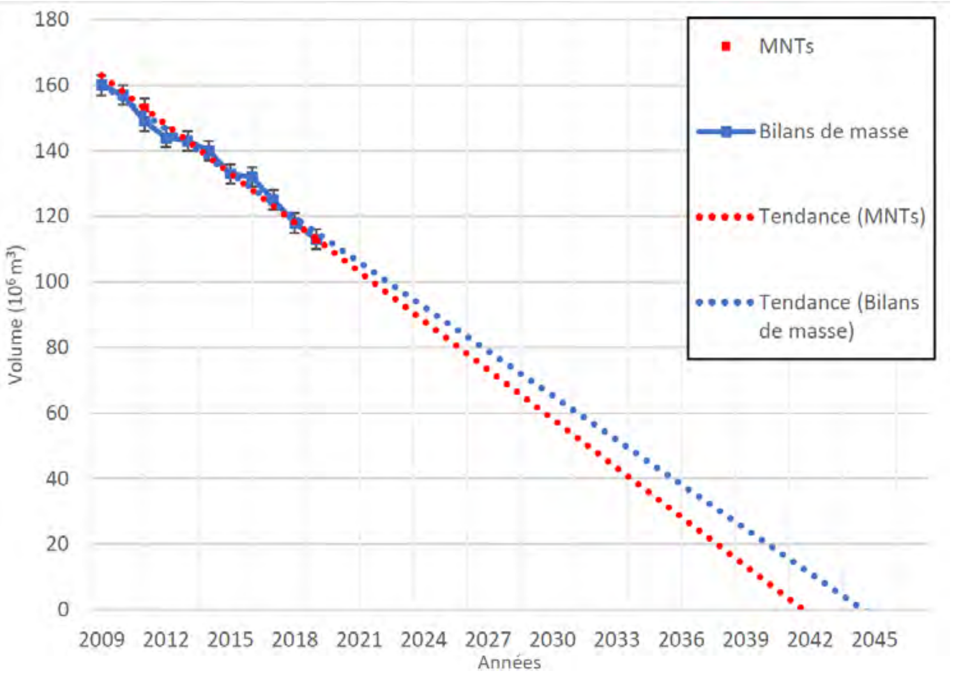

Glacier Mass balance model (Doucerain, 2021)

$$B(t_i, z) = A(t_i, z) - M(t_i, z) \qquad \text{mass balance}$$
$$A(t_i, z) = f_a \cdot P_{solid}(t_i, z) = f_a \cdot f_{solid}(T(t_i, z)) \cdot P_{total}(t_i) \qquad \text{accumulation}$$
$$M(t_i, z) = f_m \cdot \max(0, T(t_i, z) - T_{melt}) \cdot \Delta t \qquad \text{ablation/melt}$$

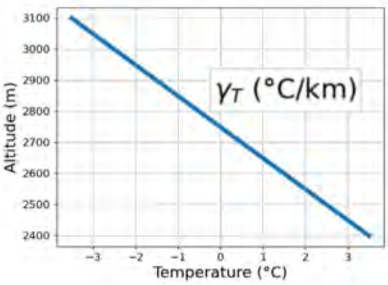

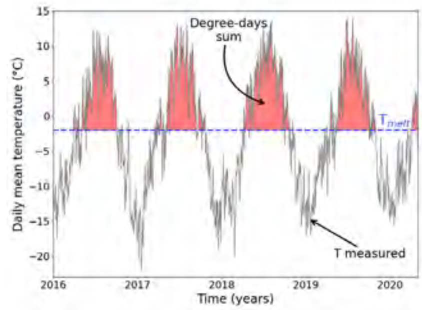

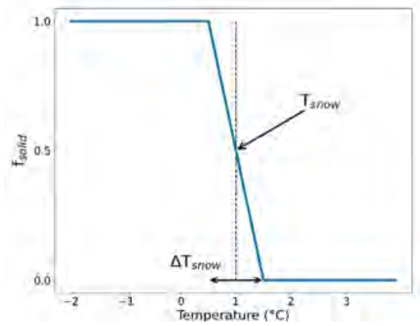

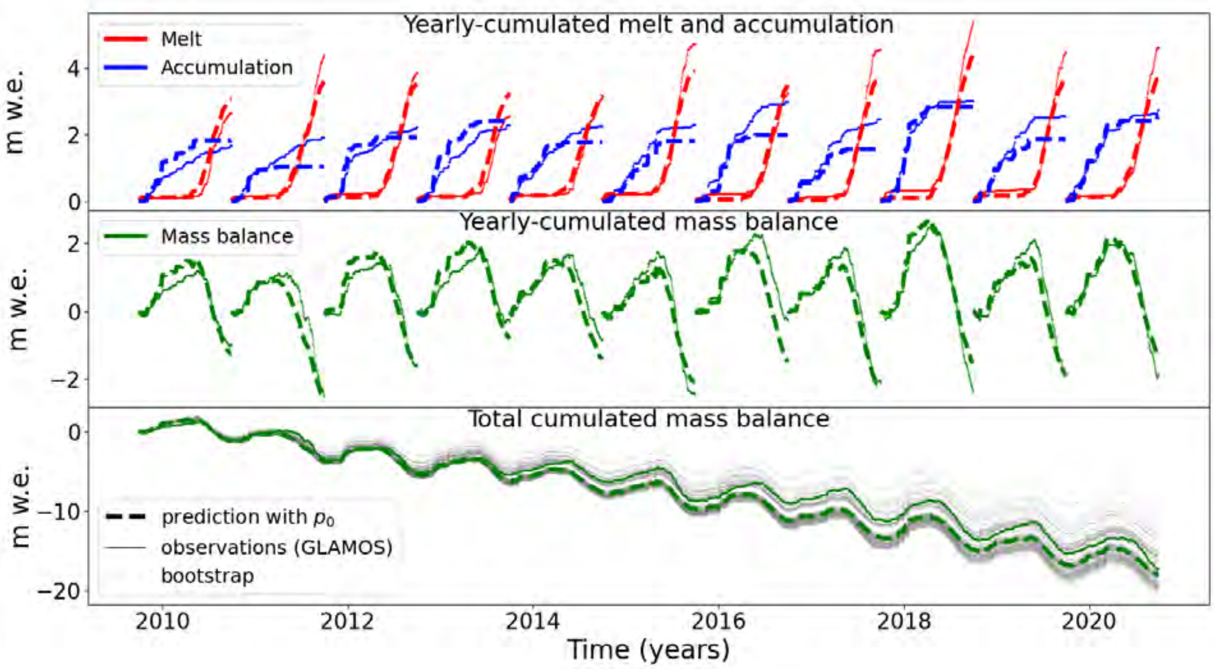

Estimated future glacier evolution under different climate scenarios using a mass-balance model (Doucerain, 2021).

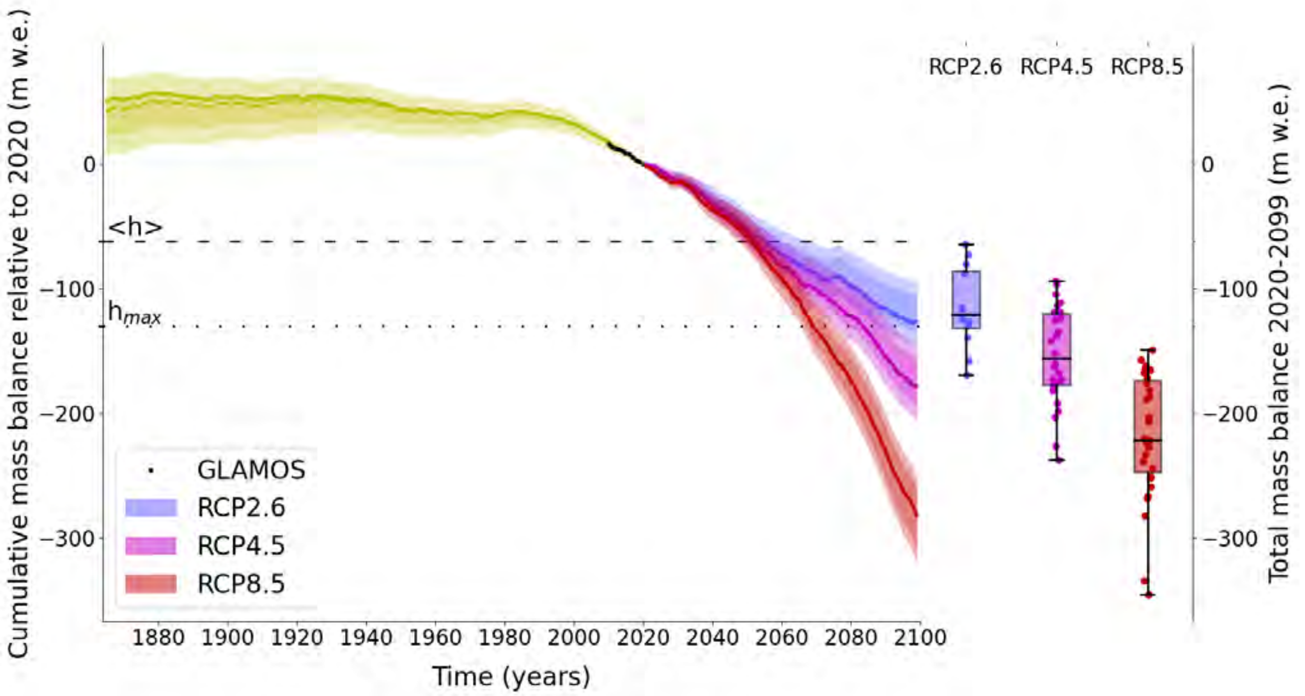

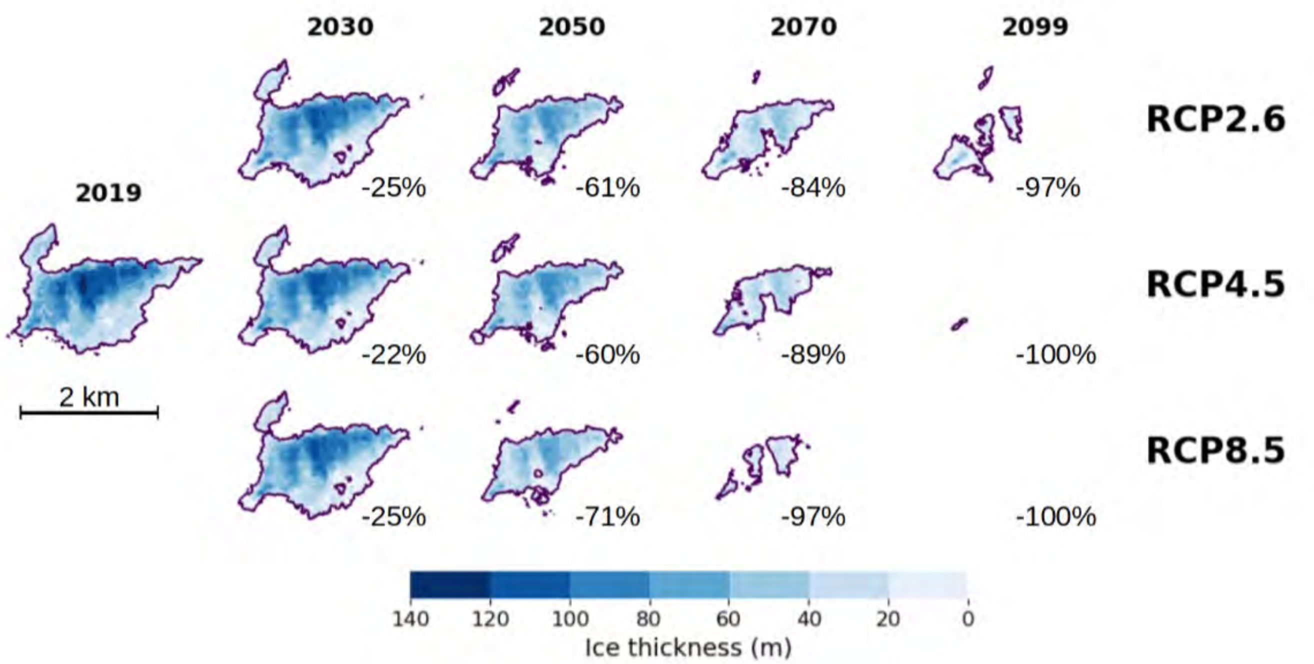

Simulated time series of the discharge of Glarey for the scenarios RCP4.5, obtained with the reservoir model developed by Salamin 2023

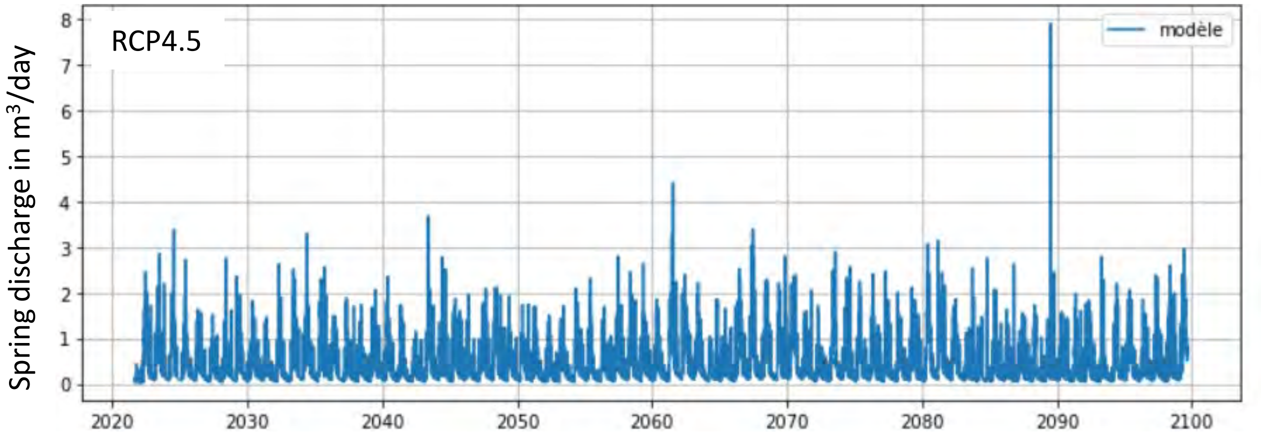

RCP4.5 - The data are smoothed using a 31-day and 15-year moving average.

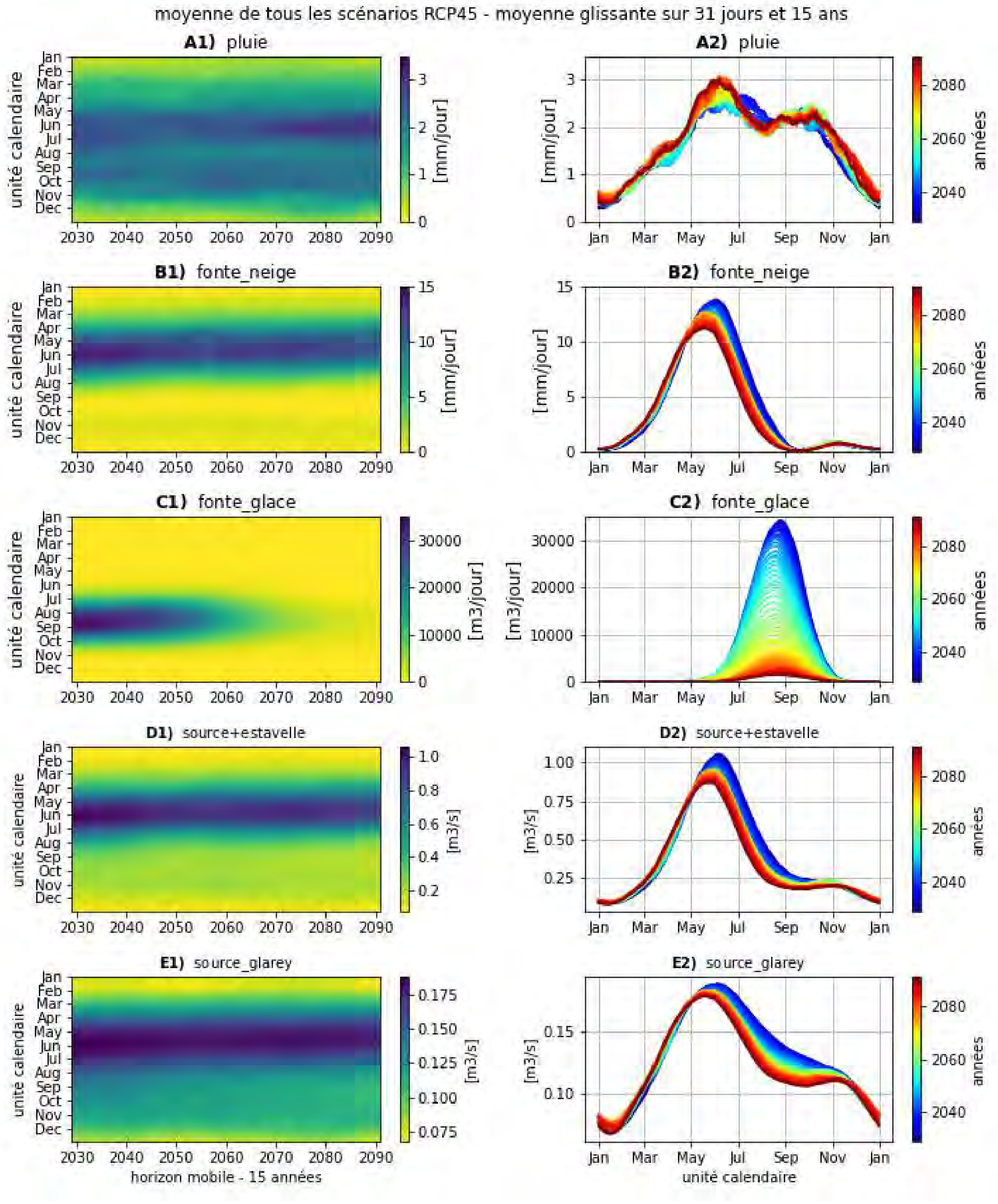

References about Tsanfleuron

Gremaud, V., Goldscheider, N., Savoy, L., Favre, G., & Masson, H. (2009). Geological structure, recharge processes and underground drainage of a glacierised karst aquifer system, Tsanfleuron-Sanetsch, Swiss Alps. Hydrogeology Journal, 17(8), 1833–1848.

Gremaud V, Goldscheider N (2010) Geometry and drainage of a retreating glacier overlying and recharging a karst aquifer, Tsanfleuron-Sanetsch, Swiss Alps. Acta Carsologica, 39(2): 289-300.

Gremaud, V. (2011). Relations between retreating alpine glaciers and karst aquifer dynamics: Tsanfleuron-Sanetsch experimental test site, Swiss Alps [Doctoral dissertation, Université de Neuchâtel, Faculté des sciences].

Neven, A., Dall'Alba, V., Juda, P., Straubhaar, J., & Renard, P. (2021). Ice volume and basal topography estimation using geostatistical methods and GPR measurements: Application on the Tsanfleuron and Scex Rouge glacier, Swiss Alps. The Cryosphere Discussions, 2021, 1-27.

Salamin, A. (2023). Site karstique de Tsanfleuron : Analyse et modélisation de la ressource en eau du bassin versant de la source de Glarey et de son évolution [Master's thesis, University of Neuchâtel, Switzerland].

Savoy, L., Favre, G., & Masotti, D. (2008). Hydrogéologie du karst de Tsanfleuron et essais multitraçages, années 2005 et 2006. Collection EDYTEM. Cahiers de géographie, 7(1), 135–146.

Tanaka, A. P. B., Renard, P., de Moraes Caldeira, J. N., & Trunz, C. (2025). Graph-based fracture network analysis to integrate structural geology properties and identify preferential flow pathways in the aquifer system of Tsanfleuron, Swiss Alps. Journal of Structural Geology, 105543.

Tanaka, A. P. B., Trunz, C., Trottet, M., Racine, T., & Renard, P. (2025). Detecting fracture networks and karst features alignments similarities in the aquifer system of Tsanfleuron, Swiss Alps (EGU25-11154). Copernicus Meetings.

Others references

Gobiet, A., Kotlarski, S., Beniston, M., Heinrich, G., Rajczak, J., & Stoffel, M. (2014). 21st century climate change in the European Alps—A review. Science of the Total Environment, 493, 1138–1151.

Hubbard, B., & Hubbard, A. (1998). Bedrock surface roughness and the distribution of subglacially precipitated carbonate deposits: Implications for formation at Glacier de Tsanfleuron, Switzerland. Earth Surface Processes and Landforms, 23(3), 261–270.

Hubbard, B., Hubbard, A., Tison, J.-L., Mader, H. M., Nienow, P., & Grust, K. (2003). Spatial variability in the water content and rheology of temperate glaciers: Glacier de Tsanfleuron, Switzerland. Annals of Glaciology, 37, 1–6.

Hubbard, B., Tison, J.-L., Janssens, L., & Spiro, B. (2000). Ice core evidence for the thickness and character of clear facies basal ice: Glacier de Tsanfleuron, Switzerland. Journal of Glaciology, 46(152), 140–150.

Paul, F., Kääb, A., Maisch, M., Kellenberger, T., & Haeberli, W. (2004). Rapid disintegration of Alpine glaciers observed with satellite data. Geophysical Research Letters, 31, L21402.

Paul, F., Kääb, A., Maisch, M., Kellenberger, T., & Haeberli, W. (2004). Rapid disintegration of Alpine glaciers observed with satellite data. Geophysical Research Letters, 31, L21402.
Zeng, C., Gremaud, V., Zeng, H., Liu, Z., & Goldscheider, N. (2012). Temperature-driven meltwater production and hydrochemical variations at a glaciated alpine karst aquifer: Implication for the atmospheric CO_2 sink under global warming. Environmental Earth Sciences, 65(8), 2285–2297.

Rispal, N., Arfib, B., Audra, P., Henry, P., Viguier, B., Zappelli, A., et al. (2026). Impact of seasonal snow on the recharge of a mountain karst aquifer under climate change: The Dévoluy case study (Southern Alps, France). Hydrology and Earth System Sciences. Under review.

Steinemann, O., Ivy-Ochs, S., Grazioli, S., Luetscher, M., Fischer, U. H., Vockenhuber, C., & Synal, H. A. (2020). Quantifying glacial erosion on a limestone bed and the relevance for landscape development in the Alps. Earth Surface Processes and Landforms, 45(6), 1401-1417.

Zeng, C., Gremaud, V., Zeng, H., Liu, Z., & Goldscheider, N. (2012). Temperature-driven meltwater production and hydrochemical variations at a glaciated alpine karst aquifer: Implication for the atmospheric CO_2 sink under global warming. Environmental Earth Sciences, 65(8), 2285–2297.